energies

MDPI

Article

Observer-Based, Robust Position Tracking in Two-Mass Drive System

Jacek Kabziński * and Przemysław Mosiołek

Institute of Automatic Control, Lodz University of Technology, 90-924 Lodz, Poland
* Correspondence: jacek.kabzinski@p.lodz.pl

Abstract: Precise motion control remains one of the most important problems in modern technology. It is especially difficult in the case of two-mass systems with flexible coupling if only the motor position and velocity are measured. We propose a new methodology of control system design in this situation. The concept is founded on a robust observer design, based on a linear matrix inequality (LMI) solution. The observer cooperates with the original nonlinear controller. The presented approach allows us to solve the position tracking problem for a two-mass drive, with unknown parameters, in the presence of disturbances (for instance, nonlinear friction-like torques) acting on both ends of the flexible shaft. Under this set of assumptions, the problem was never solved previously. The closed-loop system stability is investigated, and the uniform ultimate boundedness of state estimation errors and tracking errors is proven using Lyapunov techniques. Numerical properties of the design procedure and characteristic features of the observer, controller, and closed-loop system are demonstrated by several examples.

Keywords: electric drive; two-mass system; robust control; nonlinear control

Citation: Kabziński, J.; Mosiołek, P. Observer-Based, Robust Position Tracking in Two-Mass Drive System. *Energies* **2022**, *15*, 9093. https://doi.org/10.3390/en15239093

Academic Editors: Demba Diallo and Luigi Fortuna

Received: 18 October 2022
Accepted: 27 November 2022
Published: 30 November 2022

1. Introduction

Precise motion control remains one of the most important problems in modern technology. The accurate tracking of the desired position trajectory is required in numerous branches of industry, various areas of robot applications, transportation, medical technologies, and many fields of everyday human activity. Modern servo drives, equipped with efficient and precise electrical motors, power electronic devices, and fast microprocessor controllers acting according to advanced control algorithms, usually match all requirements of accurate motion control. The idea of perfect control is based on the ability of an electric motor control system to generate the desired torque almost without any delay or inertia. The mechanical part of the system is responsible for transmitting this propelling torque to a load machine. Usually, it is assumed that the coupling satisfies the strict assumptions

- the coupling is perfectly rigid and the position and the velocity of the load are the same as the position and the velocity of the motor shaft,
- the parameters of the load machine are known and constant,
- the acting disturbances are linear functions of state variables, for instance, viscous friction is proportional to rotational speed.

Under this hypothesis, it is possible to obtain high-quality motion tracking using standard, linear control algorithms. Unfortunately, in numerous important applications all these theoretical assumptions are substantially violated. This contribution considers such a situation, described by the following five assumptions:

(A1) load position tracking is the main control aim,
(A2) the motor is coupled with the load by a flexible shaft,
(A3) the system is modeled by ordinary differential equations, but the parameters of the shaft and of the load machine are not known exactly,

(A4) nonlinear disturbance torques are acting on both ends of the shaft independently,
(A5) only the motor position and velocity are measured.

The adopted assumptions (A1–A5) result from the analysis of practical applications. We will address their significance in the following paragraphs.

Regarding (A1) and (A2):

This type of drive is usually modeled as the so-called two-mass system. The first mass represents the motor and is connected by a flexible coupling with the load mass. The torque transmitted by the shaft consists of two components: the first part (stiffness torque) is proportional to the angle of torsion, and the second (damping torque) is proportional to the time derivative of the angle of torsion. Therefore, elastic coupling is completely characterized by two constant coefficients—the stiffness coefficient and the damping coefficient. Examples of two-mass drives can be found in numerous applications, starting from huge industrial drives with a log transmission shaft, belt, or chain, such as rolling mill drives [1], conveyer belt drives [2], cage-hoist drives [3,4], drilling rigs used in oil and gas explorations [5], some special drives used in textile [6] and paper machines [7], space antennas [8] and manipulators [9]. A major problem of such systems, limiting their performance, is the existence flow-frequency torsional vibrations. A similar phenomenon, although in higher frequencies, is observed in CNC drives [10], wind turbines [11], and microelectromechanical systems (MEMS) [12]. An important example of a two-mass drive is a robotic manipulator with flexible joints [13]. Usually, a kind of harmonic reducer transmission is applied [14]. The high-speed deformation of the flexible wheel in the harmonic reducer often increases the internal flexibility of the joint.

Although for some of the applications mentioned above, such as drilling rigs and others, speed control and attenuation of torsional oscillations is the main control problem, position tracking remains the main control aim for many others (robotic drives, CNC drives, etc.). The arguments presented above justify why assumptions (A1) and (A2) are considered.

Regarding (A3) and (A4):

A two-mass system can be modeled using several sophisticated approaches:

- distributed parameter models are used [15,16] if the shaft is long and axial, torsional, and lateral vibrations occur at the same time,
- neutral-type time-delay models [17,18] can be applied if delays connected with the oscillatory waves traveling through the shaft are significant,
- fractional order calculus [19] and some very specific techniques [20,21] can be used in special situations.

However, the majority of practically applicable controllers for two-mass drives were reported with the use of lumped parameter models, i.e., using ordinary differential equations (ODEs). The system is modeled as a mass-spring-damper, but the system parameters (especially the load inertia, stiffness, and dumping coefficients) are not known exactly, only some approximate values are available as an initial guess. Furthermore, in numerous applications, one has to consider disturbance torques acting independently at both ends of the shaft—the motor end and the load end. These disturbances, working against the motion, may be caused by friction or any other resistance caused by the load mechanism. It is rational to assume that a general, nonlinear function of the motor/load position and speed is available to model the disturbance torques, but again, the parameters are not known exactly. This reasoning explains why assumptions (A3) and (A4) are made.

Regarding (A5):

In a two-mass system, the position and the velocity of the motor end of the shaft are different then the position and the velocity of the load end. Although the load position tracking is the control aim, in numerous applications a direct measurement of the load-end shaft position and velocity is impossible. It is obvious in drilling rigs or CNC machines when the drill operates cutting a machining substance. Even if installing sensors at each end of the coupling is technically possible (as in some advanced robotic applications), numerous sensors may cause problems connected to zero drift, noise, and hysteresis, not to mention cost, fragility, and durability. Therefore, the number of sensors used is limited. This explains assumption (A5).

Control and state observations in two-mass drives have been hot research topics for many years. Although plenty of publications are available, it is difficult to find results concerning all conditions (A1–A5) considered and justified in this paper. Table 1 presents a comparison of several recently published references. The presented contribution is the only one taking all conditions (A1–A5) into account.

Of course, controller and observer designs for two-mass drives were investigated in the literature, under various assumptions, together or separately. Several active control methods were used to design controllers for two-mass systems, such as classical linear control techniques—proportional-integral (PI) control, linear-quadratic regulator (LQR), root locus, etc. [22]; artificial intelligence-based methods—artificial neural networks [23], linear model predictive control [24], fuzzy controllers [25]; nonlinear control techniques—nonlinear neural networks [26], adaptive nonlinear control [27–29], and a wave-based disturbance observer approach [30]. The majority of the described observer design methods concern load velocity observers. Among them are Luenberger observers (linear or nonlinear) [31], Kalman filters (extended, unscented) [32,33], moving horizon estimators [34], multilayer observers [35,36], LQ observers [37], and fixed gain filters (FGFs) [13]. A separate group consists of observers designed by numerous techniques inspired by artificial intelligence, but usually, the stability of such solutions was not proven.

Assumptions (A1–A5) determine that we have to cope with problems of state reconstruction (because of A5) and the tracking control (A1) for a nonlinear system (A4) with unknown parameters (A3). Therefore, an obvious technique to consider is to join an adaptive observer and an adaptive controller. This problem was investigated in [38] and it was observed that it requires the active cooperation of two adaptation mechanisms: the first acting in the observer and the other one in the controller. It is well known that adaptive observers for nonlinear systems require special conditions [39,40] and that the derivation of the stability and tuning is complicated.

Hence, in this contribution, the design is based on the nominal values of parameters and the effects of parameter mismatches and external disturbances are compensated using robust control techniques. First, the robust observer design technique is used [41]. It leads to a linear matrix inequality, which connects the observer's performance with the uncertainty constraints. Adopting this design technique makes the Luenberger-type observer the most appropriate. The observer design is presented in Section 3, and stability (in the sense of uniform ultimate boundedness of the estimation error) is established. Next, the estimated load position and speed, together with the measured motor position and speed are used to design a nonlinear tracking controller. A procedure similar to backstepping is used, with some smart modifications. The uniform ultimate boundedness of the tracking error is demonstrated using Lyapunov techniques and the bounds on the tracking error are investigated. Finally, experiments with the closed-loop system are presented and conclusions are derived.

Table 1. Recent references.

	Assumptions						
References	**(A1)**	**(A2)**	**(A3)**	**(A4)**	**(A5)**	**Approach**	**Is Stability Proven?**
[25]	Violated—speed control	Satisfied	Satisfied	Satisfied	Violated—motor and load speed are measured	Fuzzy controller with type I and type II fuzzy sets, tuned by PSO	No
[37]	Violated—speed control	Satisfied	Partially satisfied—"small" model inaccuracies	Violated—linear model	Partially satisfied—load speed estimation only	LQ technique for observer, linear controller	Yes—under assumptions of linearity

Table 1. *Cont.*

	Assumptions						
References	**(A1)**	**(A2)**	**(A3)**	**(A4)**	**(A5)**	**Approach**	**Is Stability Proven?**
[42]	Satisfied	Satisfied	Violated—known parameters	Violated—load torque proportional to the load position	Satisfied	Linear state observer and zero-order disturbance observer	Yes—under assumptions of linearity
[35,36]	Violated—speed control	Satisfied	Violated—known parameters	Violated—constant load torque	Partially satisfied—load speed estimation only	Parallel connection of the linear Luenberger observers	No
[13]	Satisfied	Satisfied	Violated—known parameters	Violated—constant load torque	Satisfied	Steady-state Kalman filter (KF), the fixed gain filter (FGF)	Yes
[31]	Violated—speed control	Satisfied	Violated—known parameters	Violated—constant load torque	Partially satisfied—load speed estimation only	Linear and nonlinear Extended State Observer (ESO) is an essential part of the Active Disturbance Rejection Control.	No
[29]	Violated—speed control	Satisfied	Satisfied	Violated—constant load torque	Violated—motor and load speed are measured	Nonlinear adaptive controller	YES
This contribution	Satisfied	Satisfied	Satisfied	Satisfied	Satisfied	Robust observer, nonlinear controller	YES

2. Plant Model and the Problem Statement

We consider a two-mass drive system modeled by ordinary differential equations

$$\begin{array}{c} \dot{x}_1 = x_2 \\ J_2\dot{x}_2 = c(x_3 - x_1) + d(x_4 - x_2) - b_2x_2 - T_{f2}(x_2) - d_2(t) \\ \dot{x}_3 = x_4 \\ J_4\dot{x}_4 = -c(x_3 - x_1) - d(x_4 - x_2) - b_4x_4 - T_{f4}(x_4) - d_4(t) + T \end{array}, \tag{1}$$

where the used symbols represent:

- J_2—the inertia of the load,
- J_4—the inertia of the motor,
- $x_1,\ x_2$—the angular position and velocity of the load,
- $x_3,\ x_4$—the angular position and velocity of the motor,
- T—the drive torque developed by the motor (the control input),
- c—the stiffness coefficient,
- d—the dumping coefficient,
- $b_2,\ b_4$—the viscous friction coefficients associated with the load and the motor, respectively,
- $T_{f2}(x_2),\ T_{f4}(x_4)$—the nonlinear friction torque associated with the load and the motor, respectively,
- $d_2(t),\ d_4(t)$—the unstructured components representing all modeling errors and external disturbances.

We assume that friction, or any other torque acting against the motion, affects both sides of the shaft. It is modeled as a linear component (ex. viscus friction) $b_ix_i,\ i = 2,4$

(which will be included into a linear part of the model) and a nonlinear, smooth, and bounded component $T_{fi}(x_i),\ i = 2,4$. Exemplary functions $T_{fi}(x_i),\ i = 2,4$ may be given by

$$T_{fi}(x_i) = \left(f_{si} + (f_{ci} - f_{si})e^{-\left(\frac{x_i}{x_{si}}\right)^2}\right)\tanh(K_i x_i); \quad i = 2,4 \tag{2}$$

representing the Stribeck effect on friction [43] and being parameterized by constant $f_{si},\ f_{ci},\ x_{si},\ K_i,\ i = 2,4$. The obtained results can be easily generalized to other forms of friction and load torque models, provided that $T_{fi},\ i = 2,4$ remain smooth and bounded functions of the state variables.

Bounded components $d_2(t),\ d_4(t)$ represent any uncertainties due to modelling errors, parameter mismatch, or external disturbances. In Equations (1)–(4), they have the character of additional load torques, not included in the parameterized components. As the modelling is as accurate as possible, it is reasonable to assume that $d_2(t),\ d_4(t)$ are bounded. Of course, motor-side parameters are usually much better known than load-side, and among them, the motor inertia J_4 is assumed to be known exactly.

Only the motor-side position and rotational speed are measured:

$$y = Gx = \begin{bmatrix} x_3 \\ x_4 \end{bmatrix} = \begin{bmatrix} 0 & 0 & 1 & 0 \\ 0 & 0 & 0 & 1 \end{bmatrix} x. \tag{3}$$

The aim of the derivation presented in this contribution is:

1. to design a robust observer able to estimate all state variables of the plant,
2. to propose a controller, which will allow sufficiently fast and accurate tracking of the desired load position $x_{1d}(t)$.

Adopting notation

$$\begin{gathered} C_1 = \tfrac{c}{J_2},\ C_2 = \tfrac{c}{J_4}, D_1 = \tfrac{d}{J_2},\ D_2(t) = \tfrac{d_2(t)}{J_2},\ D_4 = \tfrac{d}{J_4}, D_5(t) = \tfrac{d_4(t)}{J_4},\ B_2 = \tfrac{b_2}{J_2}, \\ B_4 = \tfrac{b_4}{J_4},\ T_{F2}(x_2) = \tfrac{T_{f2}(x_2)}{J_2},\ T_{F4}(x_4) = \tfrac{T_{f4}(x_4)}{J_4},\ R = \tfrac{1}{J_4}, \end{gathered} \tag{4}$$

allows us to re-write the plant model (1) in a compact form:

$$\dot{x} = Ax - F(x) + \begin{bmatrix} 0 \\ 0 \\ 0 \\ 1 \end{bmatrix} RT + D(t),\ x = \begin{bmatrix} x_1 \\ x_2 \\ x_3 \\ x_4 \end{bmatrix}, \tag{5}$$

where

$$A = \begin{bmatrix} 0 & 1 & 0 & 0 \\ -C_1 & -D_1 - B_2 & C_1 & D_1 \\ 0 & 0 & 0 & 1 \\ C_2 & D_4 & -C_2 & -D_4 - B_4 \end{bmatrix},\ F(x) = \begin{bmatrix} 0 \\ T_{F2}(x_2) \\ 0 \\ T_{F4}(x_4) \end{bmatrix},\ D(t) = \begin{bmatrix} 0 \\ D_2(t) \\ 0 \\ D_5(t) \end{bmatrix}. \tag{6}$$

As $d_i,\ T_{fi},\ i = 2,4$ are bounded functions, it is evident that $||F(x)||,\ ||D(t)||$ are bounded as well.

It is assumed that nominal, approximate values of model parameters in Equation (1) are available for the design. The subscript N denotes these values, i.e., C_{1N}, C_{2N} D_{1N}, D_{4N}, B_{2N}, B_{4N}, $T_{F2N}(x_2)$, $T_{F4N}(x_4)$ are known instead of the exact parameters used in Equations (5) and (6). Similarly, A_N and $F_N(x)$ denote values calculated, as in Equation (6) but with the use of nominal parameters.

If the parameter mismatch is considered, i.e., it is assumed that instead of the exact values of A and $F(x)$, A_N and $F_N(x)$ are available, the plant model may be represented as:

$$\begin{aligned}\dot{x} = A_N x - F_N(x) &+ \begin{bmatrix} 0 \\ 0 \\ 0 \\ 1 \end{bmatrix} RT + D_c(t) \\ &= A_N x - F_N(x) + \begin{bmatrix} 0 \\ 0 \\ 0 \\ 1 \end{bmatrix} RT + (A - A_N)x(t) - F(x(t)) \\ &+ F_N(x(t)) + D(t),\end{aligned} \tag{7}$$

where

$$\begin{aligned}&D_c(t) = \Delta A x(t) - \Delta F(x(t)) + D(t), \\ &\Delta A = A - A_N \\ &= \begin{bmatrix} 0 & 0 & 0 & 0 \\ -C_1 + C_{1N} & -D_1 + D_{1N} - B_2 + B_{2N} & C_1 - C_{1N} & D_1 - D_{1N} \\ 0 & 0 & 0 & 0 \\ C_2 - C_{2N} & D_4 - D_{4N} & -C_2 + C_{2N} & -D_4 + D_{4N} - B_4 + B_{4N} \end{bmatrix}, \\ &\Delta F_N = F - F_N = \begin{bmatrix} 0 \\ T_{F2}(x_2) - T_{F2N}(x_2) \\ 0 \\ T_{F4}(x_4) - T_{F4N}(x_4) \end{bmatrix}.\end{aligned} \tag{8}$$

As $F(x)$ is a bounded function, its nominal model $F_N(x)$ is also bounded. Therefore, for any x the difference $\Delta F_N(x) = F_N(x) - F(x)$ is bounded and for any two arguments $x,\ \hat{x}$ $F_N(x) - F_N(\hat{x})$ is bounded. As propelling torques acting in the system are limited and torques acting against the motion increase with the increasing velocities, the maximum available velocities are limited. Therefore, because of the structure of ΔA, ΔAx is bounded, and finally, $D_c(t)$ is bounded as well. The component $D_c(t)$ represents any uncertainty resulting from modelling errors, parameter mismatches, or external disturbances.

Let us denote another uncertainty-representing signal $D_p(t) = D_c(t) + F_N(\hat{x}(t)) - F_N(x(t))$, where $\hat{x}(t)$ states for the estimated state variables. $D_p(t)$ includes a mismatch due to the state estimation error, and, as explained in the previous paragraph, it is also bounded.

3. The Observer

A robust observer is proposed for system Equation (7) as a simple extension of the Luenbeger observer and the observer robustness is obtained by the LMI technique. The observer equation is

$$\dot{\hat{x}} = A_N\hat{x} - F_N(\hat{x}) + \begin{bmatrix} 0 \\ 0 \\ 0 \\ 1 \end{bmatrix} RT + LG(x - \hat{x}), \tag{9}$$

where $\hat{x}$ denotes the observer state variables and $e =: x - \hat{x}$ is the state estimation error. The matrix G, defined in Equation (3) declares that the motor speed and position are measured, while the matrix L represents the observer gains to be designed. Therefore, the estimation error dynamics is obtained by subtracting Equation (9) from Equation (7):

$$\begin{aligned}\dot{e} = \dot{x} - \dot{\hat{x}} = A_N x - F_N(x) + \begin{bmatrix} 0 \\ 0 \\ 0 \\ 1 \end{bmatrix} RT + D_c(t) - A_N\hat{x} + F_N(\hat{x}) - \begin{bmatrix} 0 \\ 0 \\ 0 \\ 1 \end{bmatrix} RT - LG(x - \hat{x}) \\ = (A_N - LG)e + D_p(t).\end{aligned} \tag{10}$$

where $D_p(t) = D_c(t) + F_N(\hat{x}(t)) - F_N(x(t))$.

The feedback-gain matrix L is designed to assure the robust stability of Equation (10). The Lyapunov function

$$V = e^T P e \tag{11}$$

with a positive definite matrix P is considered. Let us introduce three more design parameters—a symmetric matrix M and positive scalars α and ϵ, which will be used to tune the observer accuracy and robustness.

The derivative of the Lyapunov function Equation (11) along the trajectories of system (10) is given by:

$$\begin{array}{c} \dot{V} = \dot{e}^T Pe + e^T P\dot{e} = e^T (A_N - LG)^T Pe + e^T P(A_N - LG)e \\ +D_p^T(t)Pe + e^T PD_p(t). \end{array} \tag{12}$$

Hence, selecting

$$L = P^{-1} M G^T, \tag{13}$$

and adding and subtracting terms $\alpha e^T e$, $\epsilon D_p^T(t) D_p(t)$ we obtain

$$\begin{array}{c} \dot{V} = e^T A_N{}^T Pe + e^T PA_N e - e^T G^T GMe - e^T MG^T Ge + D_p^T(t)Pe + e^T PD_p(t) \\ +\alpha e^T e - \alpha e^T e - \epsilon D_p^T(t) D_p(t) + \epsilon D_p^T(t) D_p(t). \end{array} \tag{14}$$

This can be transformed into

$$\dot{V} = \gamma^T \begin{bmatrix} A_N{}^T P + PA_N - G^T GM - MG^T G + \alpha 1_4 & P \\ P & -\epsilon 1_4 \end{bmatrix} \gamma - \alpha e^T e + \epsilon D_p^T(t) D_p(t) \tag{15}$$

where $\gamma = \begin{bmatrix} e \\ D_p(t) \end{bmatrix}$ and hence, the observer stability theorem can be formulated.

Theorem 1. *If the linear matrix inequality*

$$\begin{bmatrix} A_N{}^T P + PA_N - G^T GM - MG^T G + \alpha 1_4 & P \\ P & -\epsilon 1_4 \end{bmatrix} \leq 0 \tag{16}$$

is fulfilled for a symmetric M and positive definite P, for certain $\epsilon > 0$, $\alpha > 0$, then for any uncertainty representing the component fulfilling

$$D_p^T(t) D_p(t) \leq \varepsilon_1 \tag{17}$$

the trajectories of the system (10) are ultimately uniformly bounded (UUB) [44].

Proof of Theorem 1. Indeed, under conditions (16) and (17), it follows from (15) that

$$\dot{V} \leq -\alpha e^T e + \epsilon \varepsilon_1 \ . \tag{18}$$

Hence, from (18) $\dot{V} < 0$ outside of the set $H = \left\{ e : \ e^T e \leq \frac{\epsilon \varepsilon_1}{\alpha} \right\}$, and so, the trajectories of system (10) are ultimately uniformly bounded (UUB) to the set $\widetilde{H}$—the tightest level set of $V(e)$ (11) containing the set H [44]. Moreover, the set $\widetilde{H}$ is contained in $\overline{H} = \left\{ e : \ e^T e \leq \frac{\epsilon \varepsilon_1}{\lambda_m(P)\alpha} \right\}$, where $\lambda_m(P)$ stands for the minimal eigenvalue of the symmetric matrix P. □

The presented reasoning demonstrates that the state estimation error trajectories are UUB, and indicate the impact of the parameters $\lambda_m(P)$, α, ϵ on the target set. The constraint $e^T e \leq \frac{\epsilon \varepsilon_1}{\lambda_m(P)\alpha}$ is usually very conservative and a better accuracy of the state estimation is obtained in practice, due to smart tuning.

The matrix M offers more flexibility while solving the LMI Equation (16). Although it is possible to solve Equation (16) with the pre-defined M, say $M = I$, having a symmetric M as design parameters is a smart trick to improve the obtained solution.

The quadruple of the matrices and parameters $\{M,\ P,\ \epsilon > 0, \alpha > 0\}$ fulfilling the LMI Equation (16) is not unique. To enhance the accuracy of the observer, it is necessary to select the minimal value of ϵ and the maximal value of $\lambda_m(P)$ and α among all solutions of Equation (16). If the value of ϵ decreases, the set of remaining parameters $\alpha,\ P,\ M$ fulfilling Equation (16) narrows down. Similarly, if α increases, the set of remaining parameters $\epsilon,\ P,\ M$ fulfilling Equation (16) narrows down. Finally, it may be demonstrated that the biggest eigenvalue of P, $\lambda_M(P)$, determines the speed of convergence to the target set. It is recommended that $\lambda_M(P)$ is not too high and so, the ratio ${}^{\lambda_M(P)}/_{\lambda_m(P)}$ should be as close to 1 as possible. The observer is always stable in the UUB sense, but the accuracy of the state estimation decreases if the disturbance bound ε_1 increases. The selected solution of Equation (16) decides about the important features of the observer, such as the magnitude of the observer gains.

Some numerical aspects of solving the LMI Equation (16) are presented by Example 1.

Example 1. Numerical aspects of the observer design
The data are taken from the example described in Section 4, where $A_N = \begin{bmatrix} 0 & 1 & 0 & 0 \\ -1.2647 & -0.1364 & 1.2647 & 0.0027 \\ 0 & 0 & 0 & 1 \\ 0.2229 & 0.0005 & -0.2229 & -0.2008 \end{bmatrix}$ and $G = \begin{bmatrix} 0 & 0 & 1 & 0 \\ 0 & 0 & 0 & 1 \end{bmatrix}$.
The eigenvalues of the matrix A_N are $\lambda_1 = 0$, $\lambda_2 = -0.1904$ and $\lambda_{3,4} = -0.0734 \pm 1.2172i$.

First, Nesterov and Nemirovski's projective method [45], implemented in the function mincx from the MATLAB LMI toolbox was used to minimize the ϵ subject to the LMI Equation (16) for a given $\alpha > 0$. For matrices M and P, corresponding to the minimal value of ϵ, the minimal and maximal eigenvalues of P, the Frobenius norm of the observer gain matrix $||L||$, and the bound for the ultimate state observation error $R = \frac{\epsilon\varepsilon_1}{\lambda_m(P)\alpha}$ are calculated and presented in Table 2. If the solution of the LMI Equation (16) exists, for any combination of parameters, all eigenvalues of the matrix $A_N - LG$ in the observer error Equation (10) are placed in the left half plane of the complex numbers. The distance of the closest eigenvalue to the imaginary axis d_λ is presented in the last column of the table. Although the stability of this matrix is not enough for the observer stability under disturbances and in case of unknown/changed parameters (in this case LMI Equation (16) must be satisfied), it is sufficient if we know the plant exactly ($D_p(t) = 0$ in Equation (10)).

Table 2. Minimization of the ϵ subject to LMI (16) for various values of α.

α	Minimum Value of Parameter ϵ	$\lambda_m(P)$	$\lambda_M(P)$	$\|\|L\|\|$	$R = \frac{\epsilon}{\lambda_m(P)\alpha}\varepsilon_1$	d_λ
0.1	3.7831	0.2163	3.7×10^4	$4.7 \cdot 10^4$	$174.94\varepsilon_1$	0.40
0.5	18.911	1.0536	8.3×10^4	$2.1 \cdot 10^4$	$35.897\varepsilon_1$	0.41
1		2.1808	1.2×10^5	$1.5 \cdot 10^4$	17.333	0.40
5	189.29	10.851	2.6×10^5	$6.6 \cdot 10^3$	$3.4889\varepsilon_1$	0.40
10	377.87	21.544	3.7×10^5	$4.7 \cdot 10^3$	$1.7539\varepsilon_1$	0.41
50	1892.9	109.66	8.2×10^5	$2.1 \cdot 10^3$	$0.3452\varepsilon_1$	0.39
100	3781.8	218.45	1.2×10^6	$1.5 \cdot 10^3$	$0.1731\varepsilon_1$	0.39

As shown in Table 2, increasing parameter α increases the minimum value of parameter ϵ, for which there exists a solution of the inequality Equation (16). For larger values of α, we obtain a smaller radius of the set $\overline{H}$, to which the observer's error trajectories ultimately end up. The observer gain may be reduced by constraining ${}^{\lambda_M(P)}/_{\lambda_m(P)}$, but the error bound R increases. The impact of the constraints imposed on the eigenvalues of P on $||L||$ and R is presented in Table 3. In this case, the same algorithm implemented in the function feasp was used to calculate M and P from LMI Equation (16), subject to constraints imposed on the eigenvalues of P.

Table 3. Impact of the constraints imposed on the eigenvalues of P on $||L||$ and R for $\epsilon = 100$, $\alpha = 3$.

$\lambda_{Mc}(P)$	${}^{\lambda_{Mc}(P)}/_{\lambda_{mc}(P)}$	$\lambda_m(P)$	$\lambda_M(P)$	$\|\|L\|\|$	$R = \frac{\epsilon}{\lambda_m(P)\alpha}\varepsilon_1$	d_λ
100	40	10.942	73.249	62.939	6.093 ε_1	0.18
200	40	17.219	128.8	39.845	3.872 ε_1	0.21
500	40	28.345	297.35	115.48	2.352 ε_1	0.19
500	167	24.209	289.24	140.63	2.754 ε_1	0.21
500	62.5	26.678	292.19	122.69	2.499 ε_1	0.19
500	36	22.164	311.16	703.12	3.008 ε_1	0.20

Table 4 shows the impact of the value of parameter ϵ on the solution of LMI Equation (16) for the fixed value of parameter α. Again, the function feasp was used.

Table 4. Solutions of LMI (16) for the constant $\alpha = 1$ and various ϵ.

ϵ	$\lambda_m(P)$	$\lambda_M(P)$	$\|\|L\|\|$	$\frac{\epsilon}{\lambda_m(P)\alpha}\varepsilon_1$	d_λ
1	1.3471	$6.1 \cdot 10^4$	1.4×10^4	$47.232\varepsilon_1$	0.20
2	2.3238	$8.5 \cdot 10^4$	1.1×10^4	$86.065\varepsilon_1$	0.23
5	4.7792	$1.4 \cdot 10^5$	8×10^3	$104.62\varepsilon_1$	0.26
10	9.7384	$1.9 \cdot 10^5$	5.7×10^3	$102.69\varepsilon_1$	0.26
20	22.437	$2.7 \cdot 10^5$	3.7×10^3	$89.14\varepsilon_1$	0.23
50	60.971	$4.4 \cdot 10^5$	2.1×10^3	$82\varepsilon_1$	0.21
100	126.87	$8.6 \cdot 10^5$	1.1×10^3	$78.823\varepsilon_1$	0.21

Table 4 shows that, for a constant α, an increase in ϵ reduces the value of the observer's gain matrix L. The change of parameter ϵ has a small influence on the radius of the set $\overline{H}$.

We have to remember that Nesterov and Nemirovski's projective method implemented in MATLAB function feasp, provides us with 'the most robust' solution of the LMI. It maximizes the coefficient p such that the left side of the LMI $+pI$ remains a negative definite. It may offer solutions corresponding to an unnecessary huge p and resulting in an unnecessary big $||L||$. Therefore developing some other methods, for example, minimizing the performance index which takes $||L||$ into account, may be beneficial.

The presented remarks and the example demonstrate the main rules of the observer tuning. In summary, a good robust observer design requires obtaining a balance between various requirements.

4. Tracking Controller with the Compensation of the State Estimation Errors

According to the main control aim, the system is supposed to track the desired trajectory $x_d(t)$ of the load position x_1. As the motor position and velocity are measured, the third and fourth components of the state estimation error $e = x - \hat{x} = \begin{bmatrix} e_1 & e_2 & e_3 & e_4 \end{bmatrix}$ can be used to improve the control system, while the load position and velocity must be substituted by the estimated variables obtained from the observer. The schema of the control system is presented in Figure 1.

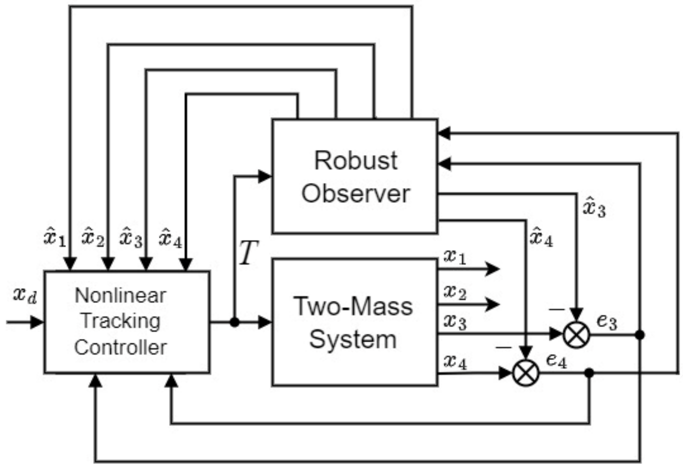

Figure 1. The control system schema.

A recurrent, step-by-step technique similar to backstepping is developed to derive the controller. At each stage, a tracking error subsystem is considered, a virtual control signal is pointed, and a Lyapunov function is investigated to propose the desired trajectory of the virtual control, such that it introduces a stabilizing term and cancels unnecessary components in the Lyapunov function derivative. Next, the virtual control tracking error is joined and the procedure is repeated. Finally, the real control is designed. The observer requires the measurement of motor speed and position while all state variables (motor position, motor speed, load position, load speed) are estimated. The nonlinear controller requires all estimated state variables and estimation errors $e_3,\ e_4$, therefore, it uses the measured motor position and speed indirectly. The main advantage of the proposed structure is that the nonlinear controller is able to react to tracking errors and observer estimation errors as well.

Stage 1.

Let us define the observer-based tracking error:

$$E_1 = x_d - \hat{x}_1 \tag{19}$$

and use Equation (9), remembering about the structure of G in Equation (3), to formulate the equation

$$\dot{E}_1 = \dot{x}_d - \dot{\hat{x}}_1 = \dot{x}_d - \hat{x}_2 - l_{11}e_3 - l_{12}e_4 \tag{20}$$

where $l_{11},\ l_{12}$ are appropriate entries of the observer gain matrix L and $e_3,\ e_4$ are appropriate components of the state estimation error e.

The error E_1 is stabilized by a proper shaping of the signal $\hat{x}_2$ (estimated load velocity obtained from the observer), which is forced to follow the desired trajectory x_{2d}. Denoting the tracking error for $\hat{x}_2$ by

$$E_2 = x_{2d} - \hat{x}_2 \tag{21}$$

provides

$$\dot{E}_1 = \dot{x}_d - x_{2d} + E_2 - l_{11}e_3 - l_{12}e_4 \tag{22}$$

The desired trajectory x_{2d} is proposed as

$$x_{2d} = \dot{x}_d + w_1E_1 \tag{23}$$

and the stabilizing gain w_1 will be derived from the Lyapunov function

$$V_1 = V + \frac{1}{2}E_1^2 \tag{24}$$

According to Equations (18) and (23), the derivative of this function along the trajectories of system (22) is given by

$$\dot{V}_1 = \dot{V} + E_1\dot{E}_1 \le -\alpha e^T e + \epsilon\varepsilon_1 + E_1(-w_1E_1 + E_2 - l_{11}e_3 - l_{12}e_4) \tag{25}$$

Selecting w_1 as

$$w_1 = k_1 + \frac{l_{11}^2 + l_{12}^2}{4r_1}, \tag{26}$$

where $k_1 > 0$ and $r_1 > 0$ are design parameters, and observing that 'completing the square technique' provides

$$\begin{aligned} -l_{11}e_3E_1 - l_{12}e_4E_1 = r_1\left(e_3^2 + e_4^2\right) - r_1\left(e_3 + \tfrac{l_{11}}{2r_1}E_1\right)^2 - r_1\left(e_4 + \tfrac{l_{11}}{2r_1}E_1\right)^2 \\ + \tfrac{l_{11}^2 + l_{12}^2}{4r_1}E_1 \end{aligned} \tag{27}$$

and allows to represent Equation (25) as

$$\begin{aligned} \dot{V}_1 \le -\alpha e^T e + \epsilon\varepsilon_1 \quad & + E_1\left(-k_1E_1 + \tfrac{l_{11}^2 + l_{12}^2}{4r_1}E_1 + E_2 - l_{11}e_3 - l_{12}e_4\right) \\ & = -\alpha e^T e + \epsilon\varepsilon_1 - k_1E_1^2 + E_1E_2 + r_1\left(e_3^2 + e_4^2\right) \\ & -r_1\left(e_3 + \tfrac{l_{11}}{2r_1}E_1\right)^2 - r_1\left(e_4 + \tfrac{l_{11}}{2r_1}E_1\right)^2 \\ & \le -(\alpha - r_1)e^T e - k_1E_1^2 + E_1E_2 + \epsilon\varepsilon_1. \end{aligned} \tag{28}$$

Under conditions that the design parameters are selected to ensure that $\alpha - r_1 > 0$, $k_1 > 0$, Equation (28) provides stability after the compensation of the terms $E_1E_2 + \epsilon\varepsilon_1$, which will be canceled in the next stage. Moreover, Equation (22) is transformed into

$$\dot{E}_1 = \ -w_1E_1 + E_2 - l_{11}e_3 - l_{12}e_4 \tag{29}$$

Stage 2.

The motion of E_2 defined in Equation (22) is given by:

$$\begin{aligned} \dot{E}_2 = \dot{x}_{2d} - \dot{\hat{x}}_2 = \ddot{x}_d + w_1\dot{E}_1 - \dot{\hat{x}}_2 = \ddot{x}_d + w_1(-w_1E_1 + E_2 - l_{11}e_3 - l_{12}e_4) \\ + C_{1N}\hat{x}_1 + (D_{1N} + B_{2N})\hat{x}_2 - C_{1N}\hat{x}_3 - D_{1N}\hat{x}_4 + F_{2N}(\hat{x}_2) - l_{21}e_3 - l_{22}e_4 \\ = \ddot{x}_d + w_1(-w_1E_1 + E_2 - l_{11}e_3 - l_{12}e_4) + C_{1N}\hat{x}_1 \\ + (D_{1N} + B_{2N})\hat{x}_2 - C_{1N}x_3 + C_{1N}e_3 - D_{1N}\hat{x}_4 + F_{2N}(\hat{x}_2) - l_{21}e_3 - l_{22}e_4 \end{aligned} \tag{30}$$

The motor position x_3 is available and is used as a virtual control stabilizing E_2. The desired trajectory for x_3 is denoted by x_{3d} and the tracking error is defined as

$$E_3 = x_{3d} - x_3 \tag{31}$$

Therefore, Equation (30) is transformed into

$$\begin{aligned} \dot{E}_2 = \ddot{x}_d + w_1(-w_1E_1 + E_2 - l_{11}e_3 - l_{12}e_4) + C_{1N}\hat{x}_1 + (D_{1N} + B_{2N})\hat{x}_2 \\ -C_{1N}x_{3d} + C_{1N}E_3 + C_{1N}e_3 - D_{1N}\hat{x}_4 + F_{2N}(\hat{x}_2) - l_{21}e_3 - l_{22}e_4 \end{aligned} \tag{32}$$

Similar techniques as used in stage 1 are applied to stabilize signals $e,\ E_1,\ E_2$. The Lyapunov function

$$V_2 = V_1 + \frac{1}{2}E_2^2 \tag{33}$$

provides

$$\begin{array}{rl}\dot{V}_2 = \dot{V}_1 + E_2\dot{E}_2 \leq & -(\alpha - r_1)e^T e - k_1 E_1^2 + E_1 E_2 + \epsilon\varepsilon_1 \\ & +E_2(\ddot{x}_d + w_1(-w_1 E_1 + E_2 - l_{11}e_3 - l_{12}e_4) + C_{1N}\hat{x}_1 \\ & +(D_{1N} + B_{2N})\hat{x}_2 - C_{1N}x_{3d} + C_{1N}E_3 + C_{1N}e_3 - D_{1N}\hat{x}_4 \\ & +F_{2N}(\hat{x}_2) - l_{21}e_3 - l_{22}e_4).\end{array} \tag{34}$$

Having in mind that x_{3d} shall provide a negative definite term concerning E_2 and compensate for unnecessary terms in Equation (34), using the square completing technique, as in stage 1, we see that selecting such x_{3d} that

$$\begin{array}{c}C_{1N}x_{3d} = \ddot{x}_d + w_2 E_2 + w_1(-w_1 E_1 + E_2) + C_{1N}\hat{x}_1 + (D_{1N} + B_{2N})\hat{x}_2 - D_{1N}\hat{x}_4 \\ +F_{2N}(\hat{x}_2) + \frac{C_{1N}^2}{2}E_2 + E_1,\end{array} \tag{35}$$

where

$$w_2 = k_2 + \frac{(w_1 l_{11} + l_{21} - C_{1N})^2 + (w_1 l_{12} + l_{22})^2}{4r_2} + \frac{C_{1N}^2}{2} \tag{36}$$

and $k_2 > 0,\ r_2 > 0$ are selected by a designer, provides

$$\begin{array}{c}\dot{E}_2 = -k_2 E_2 - \frac{(w_1 l_{11}+l_{21}-C_{1N})^2+(w_1 l_{12}+l_{22})^2}{4r_2}E_2 + w_1(-l_{11}e_3 - l_{12}e_4) + C_{1N}E_3 \\ +C_{1N}e_3 - l_{21}e_3 - l_{22}e_4 - E_1 - \frac{C_{1N}^2}{2}E_2 = -w_2 E_2 + w_1(-l_{11}e_3 - l_{12}e_4) + C_{1N}E_3 \\ +C_{1N}e_3 - l_{21}e_3 - l_{22}e_4 - E_1\end{array} \tag{37}$$

and allows to represent the Lyapunov function derivative as

$$\begin{array}{c}\dot{V}_2 = \dot{V}_1 + E_2\dot{E}_2 \leq -(\alpha - r_1)e^T e - k_1 E_1^2 + E_1 E_2 + \epsilon\varepsilon_1 \\ +E_2\left(-\frac{(w_1 l_{11}+l_{21}-C\_1N)^2+(w_1 l_{12}+l_{22})^2}{4r_2}E_2 + w_1(-l_{11}e_3 - l_{12}e_4)\right) \\ +E_2\left(-k_2 E_2 C_{1N}E_3 C_{1N}e_3 - l_{21}e_3 - l_{22}e_4 - E_1 - \frac{C_{1N}^2}{2}E_2\right) \\ = -(\alpha - r_1)e^T e - k_1 E_1^2 - k_2 E_2^2 + \epsilon\varepsilon_1 + C_{1N}E_3 E_2 - \frac{C_{1N}^2}{2}E_2^2 \\ +r_2(e_3^2 + e_4^2) - r_2\left(e_3 + \frac{w_1 l_{11}+l_{21}-C_{1N}}{4r_2}E_2\right)^2 - r_2\left(e_4 + \frac{w_1 l_{12}+l_{22}}{4r_2}E_2\right)^2 \\ \leq -(\alpha - r_1 - r_2)e^T e - k_1 E_1^2 - k_2 E_2^2 + \epsilon\varepsilon_1 + C_{1N}E_3 E_2 - \frac{C_{1N}^2}{2}E_2^2.\end{array} \tag{38}$$

Stage 3.

As expression (35) is quite complex, the exact derivative of x_{3d} is substituted by an approximate one provided by a linear filter

$$\begin{array}{c}\dot{z}_1 = z_2, \\ \dot{z}_2 = \frac{1}{a_2}(x_{3d} - z_1 - a_1 z_2).\end{array} \tag{39}$$

This technique is called the virtual control command filtering [44] or dynamic surface method [46]. The filter parameters a_1 and a_2 are selected to place the roots of the characteristic polynomial $a_2 s^2 + a_1 s + 1$ at two negative real positions to make the filter transient sufficiently fast and smooth. It is possible to select the initial conditions of the filter, such that $\rho = x_{3d} - z_1$ is bounded:

$$|\rho| = |x_{3d} - z_1| \leq \rho_m < \infty. \tag{40}$$

When the transient of system (39) is finished, $z_1 \approx x_{3d}$ and so, $z_2 \approx \dot{x}_{3d}$. Therefore, two tracking errors are considered at this stage:

$$E_3 = x_{3d} - x_3,\ \ E_{3f} = z_1 - x_3 = -(x_{3d} - z_1) + (x_{3d} - x_3) = E_3 - \rho. \tag{41}$$

It follows from Equation (39) and Equation (1), that the trajectories of E_{3f} are given by

$$\dot{E}_{3f} = \dot{z}_1 - \dot{x}_3 = z_2 - x_4 \tag{42}$$

and hence, x_4 is used as the virtual control at this stage. The desired trajectory for x_4 is denoted by x_{4d} and

$$E_4 = x_{4d} - x_4. \tag{43}$$

stands for the tracking error.

The Lyapunov function, taking into account signals $e,\ E_1,\ E_2,\ E_{3f}$, is

$$V_3 = V_2 + \frac{1}{2}E_{3f}^2\ . \tag{44}$$

Selecting x_{4d} as

$$x_{4d} = z_2 + k_3 E_{3f} + C_{1N}E_2. \tag{45}$$

where $k_3 > 0$, we are able to obtain

$$\dot{E}_{3f} = z_2 - x_{4d} + E_4 = -k_3 E_{3f} + E_4 - C_{1N}E_2. \tag{46}$$

and

$$\begin{gathered} \dot{V}_3 = \dot{V}_2 + \tfrac{1}{2}E_{3f}\dot{E}_{3f} \leq -(\alpha - r_1 - r_2)e^T e - k_1 E_1^2 - k_2 E_2^2 + \epsilon\varepsilon_1 - \tfrac{C_{1N}^2}{2}E_2^2 \\ +C_{1N}E_{3f}E_2 + C_{1N}\rho E_2 - \tfrac{C_{1N}^2}{2}E_2^2 + E_{3f}\Big(-k_3 E_{3f} + E_4 - C_{1N}E_2\Big) = \\ -(\alpha - r_1 - r_2)e^T e - k_1 E_1^2 - k_2 E_2^2 - k_3 E_{3f}^2 + E_{3f}E_4 + \epsilon\varepsilon_1 - \tfrac{1}{2}(\rho - C_{1N}E_2)^2 + \tfrac{1}{2}\rho^2 \\ \leq -(\alpha - r_1 - r_2)e^T e - k_1 E_1^2 - k_2 E_2^2 - k_3 E_{3f}^2 + E_{3f}E_4 + \epsilon\varepsilon_1 + \tfrac{1}{2}\rho_m^2 \end{gathered} \tag{47}$$

Stage 4.

Finally, we are able to use the real control T to stabilize the complete system. We start with the dynamics of the tracking error Equation (43):

$$\begin{gathered} \dot{E}_4 = \dot{x}_{4d} - \dot{x}_4 = x_{4d} - \dot{x}_4 = \dot{z}_2 + k_3\dot{E}_{3f} + C_{1N}\dot{E}_2 - C_{2N}x_1 - D_{4N}x_2 + C_{2N}x_3 \\ +(D_{4N} + B_{4N})x_4 + F_{N4}(x_4) - RT - D_{C4}(t) = \tfrac{1}{a_2}(x_{3d} - z_1 - a_1 z_2) \\ +k_3\Big(-k_3 E_{3f} + E_4 - C_{1N}E_2\Big) + C_{1N}(-w_2 E_2 + w_1(-l_{11}e_3 - l_{12}e_4) + C_{1N}E_3) \\ +C_{1N}(C_{1N}e_3 - l_{21}e_3 - l_{22}e_4 - E_1) + C_{2N}x_3 + (D_{4N} + B_{4N})x_4 + F_{N4}(x_4) \\ -C_{2N}\hat{x}_1 - C_{2N}e_1 - D_{4N}\hat{x}_2 - D_{4N}e_2 - RT - D_{C4}(t) \end{gathered} \tag{48}$$

where $D_{C4}(t)$ stands for the fourth component of uncertainty representing signal $D_C(t)$ defined in Equation (8) and is bounded: $|D_{C4}(t)| \leq D_{c4m} \leq \sqrt{\varepsilon_1}$.

Selecting the control

$$\begin{gathered} RT = \tfrac{1}{a_2}(x_{3d} - z_1 - a_1 z_2) + k_3\Big(-k_3 E_{3f} + E_4 - C_{1N}E_2\Big) + C_{1N}(-w_2 E_2 + C_{1N}E_3) \\ +C_{1N}(w_1(-l_{11}e_3 - l_{12}e_4) + C_{1N}e_3 - l_{21}e_3 - l_{22}e_4 - E_1) + C_{2N}x_3 + (D_{4N} + B_{4N})x_4 \\ +F_{N4}(x_4) - C_{2N}\hat{x}_1 - D_{4N}\hat{x}_2 + \sqrt{\varepsilon_1}\tanh\Big(\tfrac{E_4}{\mu}\Big) + w_4 E_4 + E_{3f} \end{gathered} \tag{49}$$

with

$$w_4 = k_4 + \frac{C_{2N}^2 + D_{4N}^2}{4r_3} \tag{50}$$

where the design parameters are $k_4 > 0,\ r_3 > 0,\ \mu > 0$, we are able to obtain

$$\dot{E}_4 = -k_4 E_4 - E_{3f} - \tfrac{C_{2N}^2 + D_{4N}^2}{4r_3}E_4 - C_{2N}e_1 - D_{4N}e_2 - \sqrt{\varepsilon_1}\tanh\Big(\tfrac{E_4}{\mu}\Big) - D_{C4}(t) \tag{51}$$

The final Lyapunov function, taking the complete system and the observer into account is

$$V_4 = V_3 + \tfrac{1}{2}E_4^2. \tag{52}$$

Therefore,

$$\begin{aligned}
\dot{V}_4 = \dot{V}_3 + E_4\dot{E}_4 \le -(\alpha - r_1 - r_2)e^T e - k_1E_1^2 - k_2E_2^2 - k_3E_{3f}^2 + E_{3f}E_4 + \epsilon\varepsilon_1 + \tfrac{1}{2}\rho_m^2 \\
+E_4\left(-k_4E_4 - E_{3f} - \tfrac{C_{2N}^2 + D_{4N}^2}{4r_3}E_4 - C_{2N}e_1 - D_{4N}e_2 - \sqrt{\varepsilon_1}\tanh\left(\tfrac{E_4}{\mu}\right) - D_{C4}(t)\right) = \\
-(\alpha - r_1 - r_2)e^T e - k_1E_1^2 - k_2E_2^2 - k_3E_{3f}^2 - k_4E_4^2 + \epsilon\varepsilon_1 + \tfrac{1}{2}\rho_m^2 + r_3\left(e_1^2 + e_2^2\right) \\
-r_3\left(e_1 + \tfrac{C_{2N}}{2r_3}E_4\right)^2 - r_3\left(e_2 + \tfrac{D_{4N}}{2r_3}E_4\right)^2 - \sqrt{\varepsilon_1}E_4\tanh\left(\tfrac{E_4}{\mu}\right) - E_4D_{C4}(t)
\end{aligned} \tag{53}$$

and this provides the inequality

$$\begin{aligned}
\dot{V}_4 \le -(\alpha - r_1 - r_2 - r_3)e^T e - k_1E_1^2 - k_2E_2^2 - k_3E_{3f}^2 - k_4E_4^2 + \epsilon\varepsilon_1 + \tfrac{1}{2}\rho_m^2 \\
-\sqrt{\varepsilon_1}E_4\tanh\left(\tfrac{E_4}{\mu}\right) + \sqrt{\varepsilon_1}|E_4| - \sqrt{\varepsilon_1}|E_4| + |E_4||D_{C4}(t)|.
\end{aligned} \tag{54}$$

Using the well-known inequality $0 \le |u| - u\tanh\left(\frac{u}{\mu}\right) \le 0.278\mu$ [47] simplifies Equation (54) into

$$\begin{aligned}
\dot{V}_4 \le -(\alpha - r_1 - r_2 - r_3)e^T e - k_1E_1^2 - k_2E_2^2 - k_3E_{3f}^2 - k_4E_4^2 \\
+\epsilon\varepsilon_1 + \tfrac{1}{2}\rho_m^2 + 0.278\mu\sqrt{\varepsilon_1}.
\end{aligned} \tag{55}$$

This derivation can be concluded by the following theorem.

Theorem 2. *If the positive design parameters α, ϵ (for the observer) and $k_1, k_2, k_3, k_4, r_1, r_2, r_3, \mu$ (for the controller) are selected to fulfill the condition*

$$\alpha - r_1 - r_2 - r_3 > 0, \tag{56}$$

the trajectories of the state vector $\vartheta = \left[e\ E_1\ E_2\ E_{3f}\ E_4\right]^T$ are uniformly ultimately bounded (UUB).

Proof of Theorem 2. Indeed, it follows from (55) that $\dot{V}_4 < 0$ outside a compact set $D = \left\{\vartheta :\ \vartheta^2 \le \frac{\Omega}{K_m}\right\}$, where $\Omega = \epsilon\varepsilon_1 + \frac{1}{2}\rho_m^2 + 0.278\mu\sqrt{\varepsilon_1}$ and $K_m = \min\{\alpha - r_1 - r_2 - r_3, k_1, k_2, k_3,\ k_4\ \}$, so the trajectories of ϑ are ultimately uniformly bounded (UUB) to the tightest level set of $V_4(\vartheta)$ containing the set D [44].

Moreover, it is possible to reduce the volume of D by increasing K_m, i.e., increasing $\alpha, k_1, k_2, k_3,\ k_4$. □

The obtained result concerns the tracking gap $E_1 = x_{1d} - \hat{x}_1$ between the desired load position and the estimated load position obtained from the observer. The main aim of the controller is to diminish the tracking error $x_{1d} - x_1$ between the desired and real load position. Considering that

$$|x_{1d} - x_1| = |x_{1d} - \hat{x}_1 + \hat{x}_1 - x_1| = |E_1 - e_1| \le |E_1| + |e_1| \tag{57}$$

and that both E_1 and e_1 are UUB proves that also $x_{1d} - x_1$ is UUB.

Further investigation of Equation (55) allows to write down:

$$\begin{aligned}\dot{V}_4 \leq -(\alpha - r_1 - \quad & r_2 - r_3)e^T e - k_1 E_1^2 - k_2 E_2^2 - k_3 E_{3f}^2 - k_4 E_4^2 + \Omega \\ & \leq -\left(\tfrac{\alpha - r_1 - r_2 - r_3}{\lambda_M(P)}\right) e^T \lambda_M(P) e - k_1 E_1^2 - k_2 E_2^2 - k_3 E_{3f}^2 \\ & -k_4 E_4^2 \leq -2\gamma_m \tfrac{1}{2}\left(2e^T P e + E_1^2 + E_2^2 + E_{3f}^2 + E_4^2\right) + \Omega \\ & = -k_m V_4 + \Omega\end{aligned} \tag{58}$$

where

$$\gamma_m = \min\left\{\frac{\alpha - r_1 - r_2 - r_3}{2\lambda_M(P)},\ k_1,\ k_2, k_3, k_4\right\},\ k_m = 2\gamma_m. \tag{59}$$

The inequality (58) is the initial point to the series of transformations:

$$\begin{gathered} e^{k_m t}\dot{V}_4 \leq -k_m e^{k_m t} V_4 + e^{k_m t}\Omega \\ \tfrac{d}{d\tau}\left[e^{k_m \tau} V_4\right] \leq e^{k_m t}\Omega \\ \int_0^t \tfrac{d}{d\tau}\left[e^{k_m \tau} V_4(\tau)\right] d\tau \leq \int_0^t e^{k_m \tau}\Omega d\tau \\ e^{k_m t} V_4\Big|_0^t \leq \ e^{k_m t}\tfrac{\Omega}{k_m}\Big|_0^t \\ e^{k_m t} V_4 - V_4(0) \leq \tfrac{\Omega}{k_m}\left(e^{k_m t} - 1\right) \\ V_4(t) \leq e^{-k_m t} V_4(0) + \tfrac{\Omega}{k_m}\left(1 - e^{-k_m t}\right)\end{gathered} \tag{60}$$

Using the last inequality, we obtain

$$\frac{1}{2}\lambda_m(P) e_1^2 \leq \frac{1}{2}\lambda_m(P) e^T e \leq \frac{1}{2} e^T P e \leq V_4 \leq e^{-k_m t} V_4(0) + \frac{\Omega}{k_m}\left(1 - e^{-k_m t}\right) \tag{61}$$

and

$$\frac{1}{2}E_1^2 \leq V_4 \leq e^{-k_m t} V_4(0) + \frac{\Omega}{k_m}\left(1 - e^{-k_m t}\right). \tag{62}$$

As $E_1^2 + 2e_1 E_1 + e_1^2 \geq 0$ and $(x_{1d} - x_1)^2 = (E_1 - e_1)^2 = E_1^2 - 2e_1 E_1 + e_1^2 \leq E_1^2 - 2e_1 E_1 + e_1^2 + E_1^2 + 2e_1 E_1 + e_1^2 = 2\left(E_1^2 + e_1^2\right)$, inequalities (59) and (60) result in

$$\begin{aligned}(x_{1d} - x_1)^2 \leq 2 \quad & \left(E_1^2 + e_1^2\right) \\ & \leq e^{-k_m t} V_4(0) + \tfrac{\Omega}{k_m}\left(1 - e^{-k_m t}\right) \\ & + \tfrac{1}{\lambda_m(P)}\left(e^{-k_m t} V_4(0) + \tfrac{\Omega}{k_m}\left(1 - e^{-k_m t}\right)\right) \\ & \leq e^{-k_m t}\left(V_4(0) + \tfrac{V_4(0)}{\lambda_m(P)}\right) + \left(\tfrac{\Omega}{k_m} + \tfrac{\Omega}{\lambda_m(P) k_m}\right)\left(1 - e^{-k_m t}\right).\end{aligned} \tag{63}$$

So, for $t \to \infty$

$$\lim_{t \to \infty}|x_{1d} - x_1| \leq \sqrt{\frac{\Omega}{k_m} + \frac{\Omega}{\lambda_m(P) k_m}}. \tag{64}$$

The inequalities (63) and (64) derived here may be too conservative to provide practical constraints for the tracking error, but they clearly indicate the influence of the design parameters on the transient and quasi-steady-state behavior of the tracking error.

In Figure 2, the schema of the proposed controller is presented. The procedure for tuning the controller parameters is shown in Figure 3.

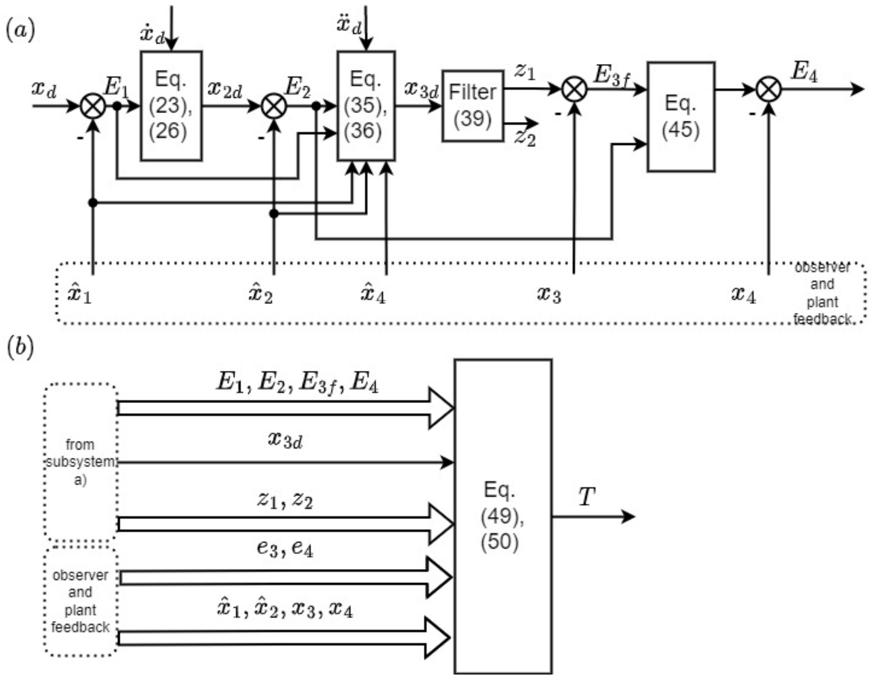

Figure 2. Diagram of the controller: (**a**) preparation of the auxiliary signals, (**b**) the control signal.

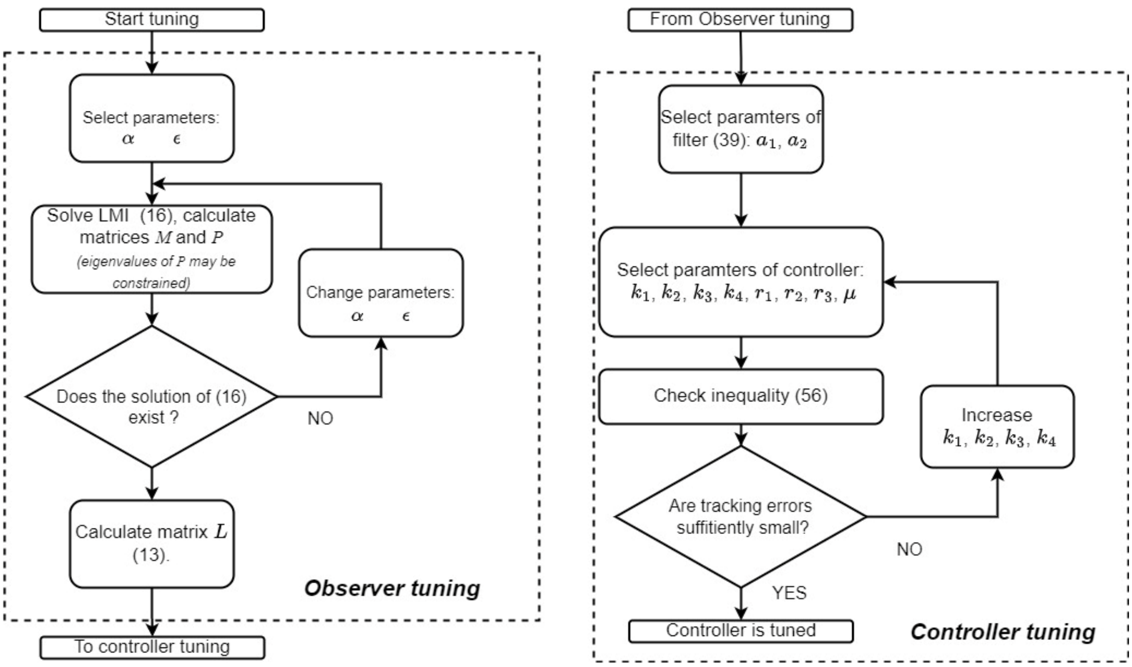

Figure 3. The procedure for tuning the controller parameters.

5. Results

The distinctive features of the proposed approach are investigated by a simulation of a drive with load and motor inertia $J_2 = 374\ \left[kg\ m^2\right],\ \ J_4 = 2122\ \left[kg\ m^2\right]$. Such big values are typical for huge manipulators used in heavy industries. The parameter J_4 contains not only the motor but also the so-called rotary table. A simplified diagram of such a device, used to manipulate objects in a huge CNC machine is shown in Figure 4.

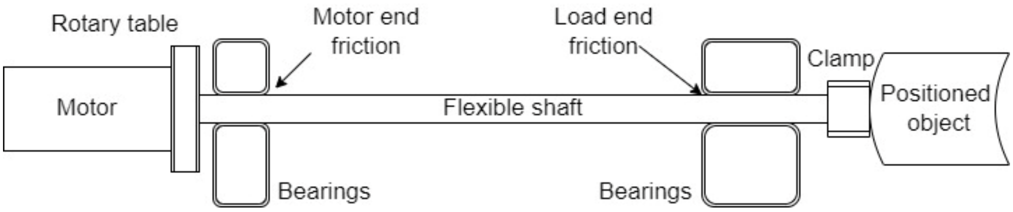

Figure 4. Schematic diagram of a drive with an elastic coupling.

The friction torques of the motor T_4 and load T_2 are described by

$$T_i(x_i) = b_i x_i + T_{fi}(x_i), \quad T_{fi}(x_i) = \left(f_{si} + (f_{ci} - f_{si}) e^{-\left(\frac{x_i}{x_{si}}\right)^2} \right) \tanh(K_i x_i); \quad i = 2, 4. \tag{65}$$

The parameters in Equation (65) are: $b_4 = 50 \left[\frac{Nms}{rad}\right]$, $b_2 = 425 \left[\frac{Nms}{rad}\right]$, $f_{s4} = 150\ [Nm]$, $f_{c4} = 400\ [Nm]$, $f_{s2} = 15\ [Nm]$, $f_{c2} = 24\ [Nm]$, $x_{s2} = x_{s4} = 0,1 \left[\frac{rad}{s}\right]$, $K_2 = K_4 = 100\ \left[\frac{s}{rad}\right]$. The stiffness and damping parameters of the shaft are: $c = 473 \left[\frac{Nm}{rad}\right]$, $d = 1 \left[\frac{Nm \cdot s}{rad}\right]$. The exact value of matrix A is:

$$A = \begin{bmatrix} 0 & 1 & 0 & 0 \\ -1.2647 & -0.1364 & 1.2647 & 0.0027 \\ 0 & 0 & 0 & 1 \\ 0.2229 & 0.0005 & -0.2229 & -0.2008 \end{bmatrix} \tag{66}$$

The step response of the motor speed and the load speed is shown in Figure 5. At $t = 100\ [s]$, f_{s2} , f_{c2} were multiplied by 10/3. We can observe the oscillatory character of the two-mass resonant systems. As the moments of inertia J_4, J_2 are quite big, the plant is rather slow. The strongly nonlinear friction also contributes to high amplitude oscillations visible during the first 40 s of the step response. In Figure 6, the open loop position control is presented. The drive is started with constant torque $T = 550\ [Nm]$. At time $t = 40\ [s]$ the value of the propelling torque T was changed to zero. Torsional vibrations are visible in both cases—in Figures 5 and 6, during the starting and braking phases. The oscillatory shaft twisting is visible in plots of the torsion angle. Of course, it is an unacceptable phenomenon and will be eliminated by the proposed controller.

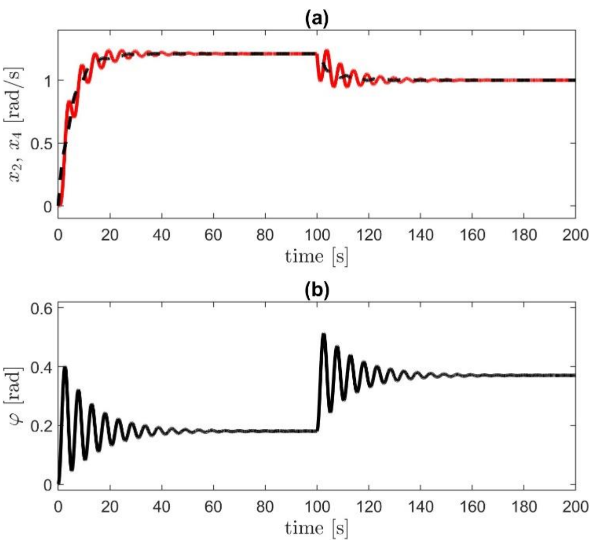

Figure 5. Step response of the motor speed and the load speed, $T = 1000\ [N]$: (**a**) load speed x_2 (solid red line) and motor speed x_4 (dashed black), (**b**) torsion angle $\varphi = x_3 - x_1$.

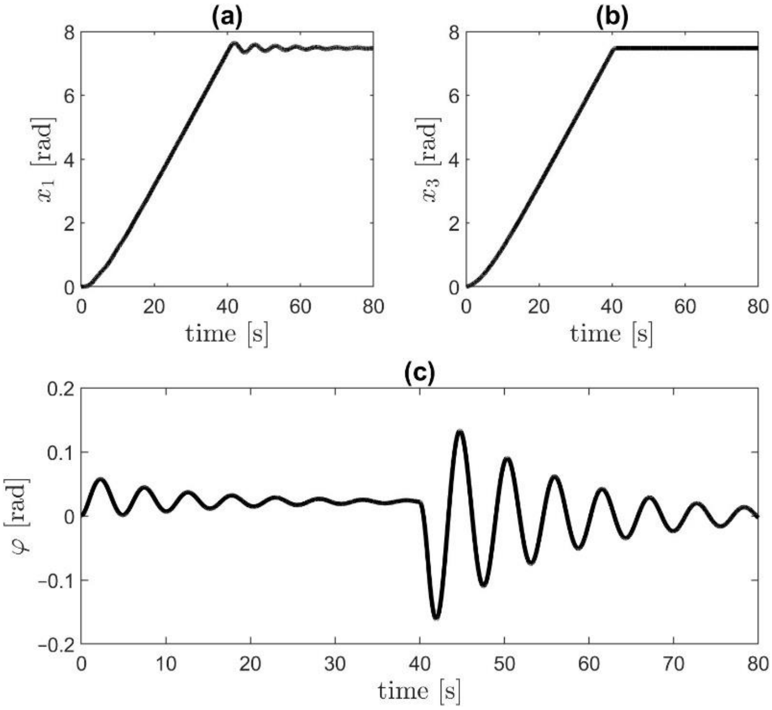

Figure 6. Open loop position control: (**a**) load position x_1, (**b**) motor position x_2, (**c**) torsion angle $\varphi = x_3 - x_1$.

Simulation examples, selected from many performed, are presented below. In the first example, the properties of the proposed robust observer were checked. The second example presents the results of the designed control algorithm.

5.1. Example 2—Observer Performance

First, the features of the observer proposed in Section 2 are presented. The tuning of the observer begins with selecting parameters α and ϵ and solving inequality (16). The gain matrix L is calculated from Equation (13).

In the first experiment, the influence of the design parameters on the performance of the observer was checked. The initial conditions for the observer were selected as $\hat{x}(0) = [1\ 0\ 1\ 0]^T$ and for the two mass system as $x = [0\ 0\ 0\ 0]^T$. The constant torque $T = 2000$ $[Nm]$ is applied. It was assumed that all plant parameters are known, so the nominal matrix A_N was equal to the true matrix A. The tests were carried out for three values of the parameter α: $\alpha_1 = 1$; $\alpha_2 = 3$ and $\alpha_3 = 7$, while ϵ remains constant $\epsilon = 100$. Following the solution of LMI (16), the gain matrices L were obtained:

$$L_1 = \begin{bmatrix} 0 & 498 \\ 37.9 & -6.3 \\ 69 & 30 \\ -6.7 & 179 \end{bmatrix};\ L_2 = \begin{bmatrix} 0 & 1169 \\ 12.6 & 437 \\ 69 & 10 \\ -2.2 & 186 \end{bmatrix};\ L_3 = \begin{bmatrix} 0 & 1870 \\ 10 & 1568 \\ 16 & 1 \\ -0.22 & 4.4 \end{bmatrix} \tag{67}$$

The results of the experiment are shown in Figure 7. All errors converge to zero, so $\hat{x} \to x$. The proposed observer provides the perfect estimation of state variables x if the exact parameters of the plant are known. A faster error convergence is obtained for higher values of parameter α.

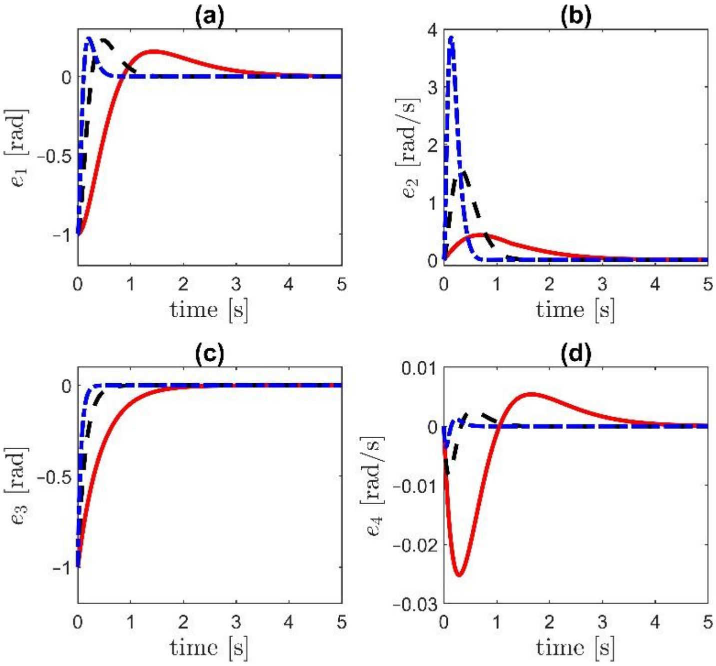

Figure 7. Observer errors e_1 (**a**), e_2 (**b**), e_3 (**c**), and e_4 (**d**). Dashed blue line—$\alpha = 7$, dash-dotted black line—$\alpha = 3$, solid red line—$\alpha = 1$.

In the second experiment, the observer robustness was tested against the parametric uncertainty. The observer errors e_1 and e_2 are shown in Figure 8 for two different values of parameters α. The observer is started knowing the actual values of parameters J_1, J_2, f_{s4}, f_{c4}, f_{s2}, f_{c2}, x_{s2}, and x_{s4}. The real parameters c, d, b_2, and b_4 used in the observer were equal to 110% of the nominal parameters. The constant torque $T = 2000$ $[Nm]$ was applied. At $t = 60$ $[s]$, the actual value of J_2 (load inertia) was increased to 120% of the nominal value ($J_2 = 449$ $\left[kg\ m^2\right]$). Finally, at $t = 120$ $[s]$, the actual f_{s2} and f_{c2} (load-end friction parameters) were increased to 120% of the nominal values ($f_{s2} = 18$ $[Nm]$, $f_{c2} = 29$ $[Nm]$). The initial conditions of the observer and the drive were equal.

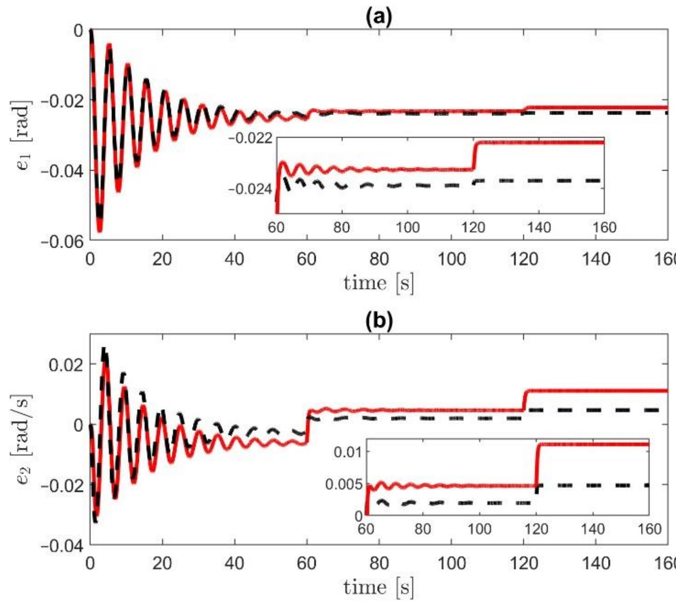

Figure 8. Influence of the parameter changes on observer error e_1 (**a**) and e_2 (**b**). Dashed black line—$\alpha = 7$, solid red line—$\alpha = 5$.

The proposed observer is working correctly. The influence of the plant parameter changes is stronger if the design parameter α is smaller. For a wide range of parameter changes, the proposed observer is stable in the UUB sense, the steady-state errors are small (less than 0.25% of the steady-state values), and will be compensated by the nonlinear tracking controller.

5.2. Example 2—Closed-Loop System Performance

The closed-loop system is designed, starting with the selection of parameters α and ϵ. Next, the LMI Equation (16) is solved and therefore the observer is designated. The design of the controller requires the selection of the parameters of the filter—a_1 and a_2 Equation (39), and next, the controller parameters $k_1, k_2, k_3,\ k_4, r_1, r_2, r_3, \mu$ must be adjusted, having in mind inequality (56). The gains $k_1, k_2, k_3,\ k_4$ are especially important, as they influence the speed of convergence and the quasi-steady-state behavior of the tracking errors.

For all presented experiments, the observer was designed using $\alpha = 0.5$ and $\epsilon = 300$. The gain matrix L was calculated from Equation (13)

$$L = \begin{bmatrix} 0 & 223.4 \\ 1.2647 & 231.04 \\ 4.6 & 1 \\ -0.2229 & 12263 \end{bmatrix} \tag{68}$$

The filter parameters in Equation (39) are $a_1 = 0.02$ and $a_2 = 10^{-4}$. The controller parameters $r_1 = r_2 = r_3 = 0.05, \mu = 0.01$ are constant, while a few variants of the gains $k_1, \ldots, k_4$ are tested.

During the first experiment, the position tracking of a continuous reference trajectory is studied. The desired position is $x_{1d} = 0.3\sin(0.3t)$. The observer initial condition is $\hat{x}(0) = [0\ 0\ 0\ 0]^T$ and the drive initial condition is $x(0) = [0.3\ 0\ 0\ 0]^T$.

Nominal values of parameters J_2, $f_{s2,}$ and f_{c2} are equal to 120% of the true values. Other parameters are known exactly. The results of the experiments are shown in Figures 7–9.

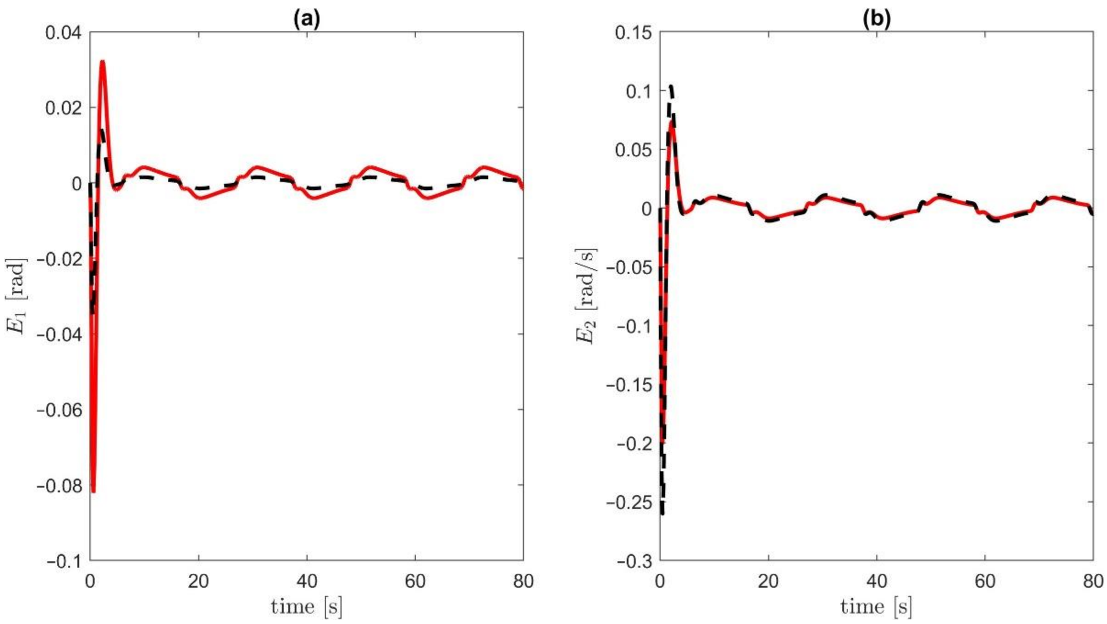

Figure 9. (**a**) Tracking error E_1, (**b**) tracking error E_2. Dashed black line—$k_1 = k_2 = k_3 = k_4 = 15$, solid red line—$k_1 = k_2 = k_3 = k_4 = 5$.

Figure 9 demonstrates the internal controller tracking errors $E_1 = x_d - \hat{x}_1$ and $E_2 = x_{2d} - \hat{x}_2$ for the different values of control parameters $k_1, \ldots, k_4$. Filtered error E_{3f}

and error E_4 are shown in Figure 10 (only initial and quasi-steady state parts of the time history are presented in Figure 10b). The proposed controller is working correctly in a wide range of controller gains $k_1, \ldots, k_4$. The internal signals of the controller are UUB. For the bigger values of parameters k_i the steady-state tracking errors E_i are smaller.

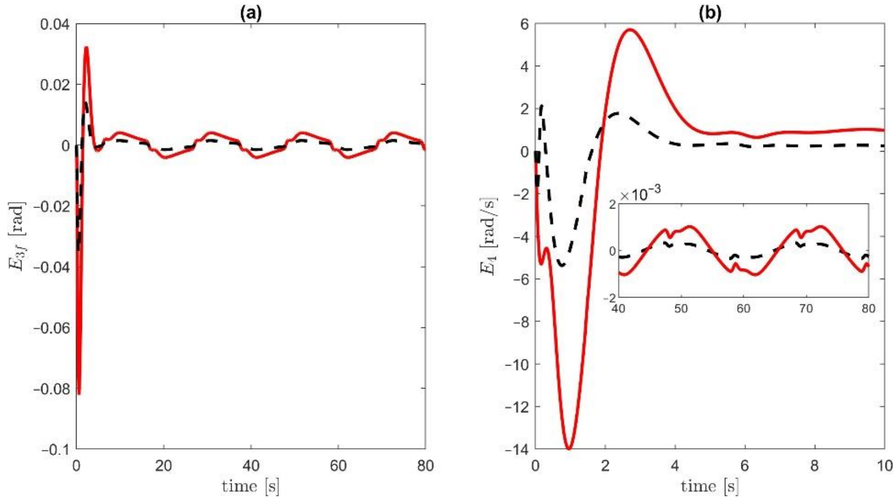

Figure 10. (**a**) Tracking error E_{3f}, (**b**) tracking error E_4. Dashed black line—$k_1 = k_2 = k_3 = k_4 = 15$, solid red line—$k_1 = k_2 = k_3 = k_4 = 5$.

Of course, the control aim is to minimize the tracking errors $x_{1d} - x_1$ and $\dot{x}_{1d} - x_2$. It is demonstrated in Figure 11 (again, only initial and quasi-steady state parts of the plots are presented) that these tracking errors are sufficiently small (quasi-steady state error amplitude is smaller than 1.7% of the reference amplitude) and increasing gains $k_1, \ldots, k_4$ of the controller reduces the quasi-steady state errors. In the interval $[40,\ 80][s]$, both the mean and the extremal quasi-steady state error for $k_1 = k_2 = k_3 = k_4 = 15$ (solid red line in Figure 11) are evidently smaller than for $k_1 = k_2 = k_3 = k_4 = 5$ (dashed black line in Figure 11).

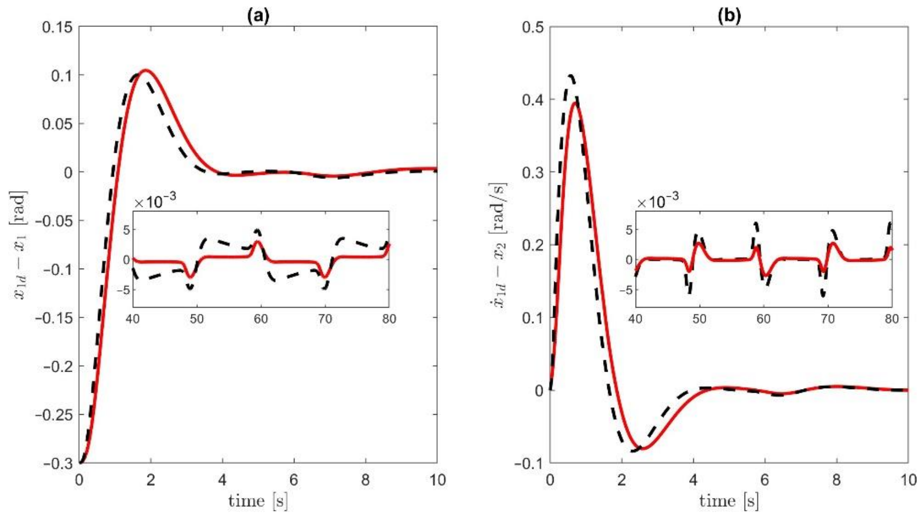

Figure 11. (**a**) Tracking error $x_{1d} - x_1$, (**b**) tracking error $\dot{x}_{1d} - x_2$. Dashed black line—$k_1 = k_2 = k_3 = k_4 = 5$, solid red line—$k_1 = k_2 = k_3 = k_4 = 15$.

The reference $x_{1d} = 0.3\sin(\omega t),\ \omega = 0.3 \left[\frac{rad}{s}\right]$ results in the reversal motion between $[-0.3,\ 0.3]\ [rad]$ with the speed in the range $[-0.09,\ 0,09]\ \left[\frac{rad}{s}\right]$. Although the quasi-steady state tracking error is small $|x_{1d} - x_1| < 10^{-3}\ [rad]$, the extrema of this error occur close to extremal values of x_{1d}, so, when the desired speed is close to zero. To check the impact of the variable desired speed on the accuracy of tracking, the same experiment was repeated with different values of ω. Two quality measures were used to evaluate the operation of the control system during the transient: the maximum absolute error (MAE) and integral squared error (ISE). Results are presented in Table 5. It may be observed that bigger ω (faster reversal motion) results in a bigger MAE and ISE, while the quasi-steady state tracking error remains at the same level.

Table 5. Comparison of the quality indices ISE and MAE for the different values of ω.

ω	ISE($x_{1d}-x_1$)	MAE($x_{1d}-x_1$)	ISE($\dot{x}_{1d}-x_2$)	MAE($\dot{x}_{1d}-x_2$)
0.6	0.0023	0.008	0.0017	0.01
0.4	0.0008	0.005	0.0007	0.008
0.2	0.0006	0.003	0.0003	0.005
0.1	0.0005	0.002	0.0001	0.003
0.05	0.0004	0.0015	0.00007	0.001

In the second experiment, the main control aim is to follow the desired position trajectory shown in Figure 12. Initially, the reference position x_{1d} starts from 0 to $0.2[rad]$. At $t = 10$ $[s]$, x_{1d} is changed from $0.2[rad]$ to $0.1[rad]$. Next, at $t = 20$ $[s]$, x_{1d} is changed from $0.1[rad]$ to $-0.2[rad]$. For the end, at $t = 30$ $[s]$, x_{1d} is changed from $-0.2[rad]$ to $0[rad]$.

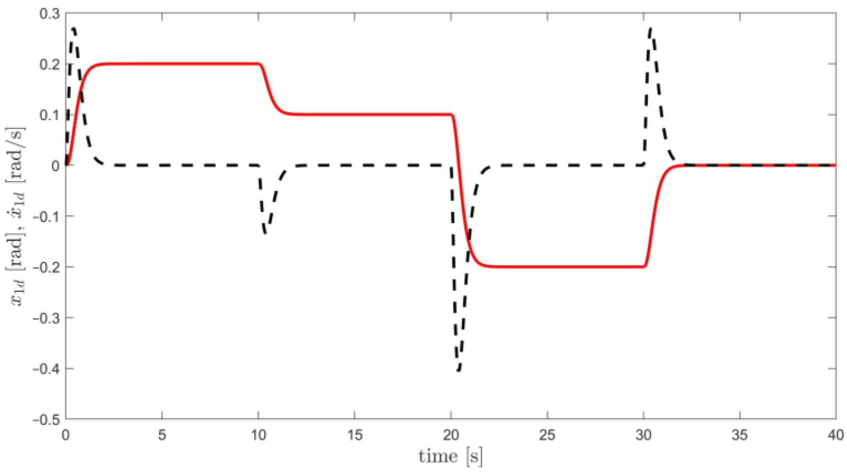

Figure 12. The desired trajectory x_{1d} (solid red line) and derivative $\dot{x}_{1d}$ (dashed black line).

Figure 13 demonstrates the tracking errors $E_1 = x_d - \hat{x}_1$ and $E_2 = x_{2d} - \hat{x}_2$ for different values of control parameters $k_1, \ldots, k_4$. The tracking errors $x_{1d} - x_1$ and $\dot{x}_{1d} - x_2$. are demonstrated in Figure 14—again only the initial and quasi-steady state parts of the plots are presented. In the interval $[10,\ 40][s]$, both, the mean and the extremal quasi-steady state error for $k_1 = k_2 = k_3 = k_4 = 15$ (solid red line in Figure 14) are evidently smaller than for $k_1 = k_2 = k_3 = k_4 = 5$ (dashed black line in Figure 14), so increasing the gains $k_1, \ldots, k_4$ reduces the quasi-steady state errors. Despite the rapid changes in the desired speed $\dot{x}_{1d}$ presented in Figure 12, the proposed controller offers a fast response to any change of the reference and a small steady-state error. The control system is stable. The torsional oscillations of the shaft are eliminated. Good tracking and transient performances are maintained, although the desired trajectory is not smooth at the isolated points.

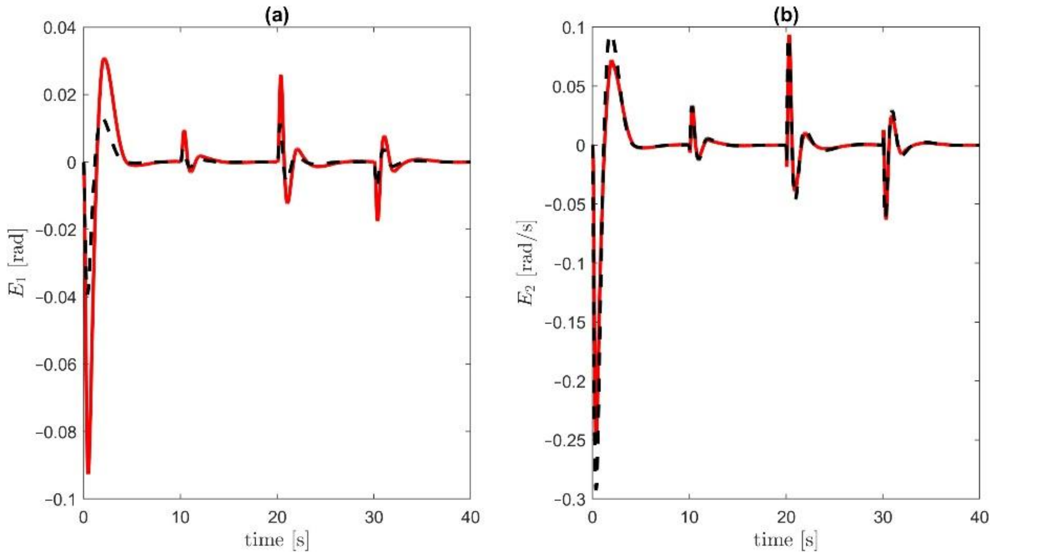

Figure 13. (**a**) Tracking error E_1, (**b**) tracking error E_2. Dashed black line—$k_1 = k_2 = k_3 = k_4 = 5$, solid red line—$k_1 = k_2 = k_3 = k_4 = 15$.

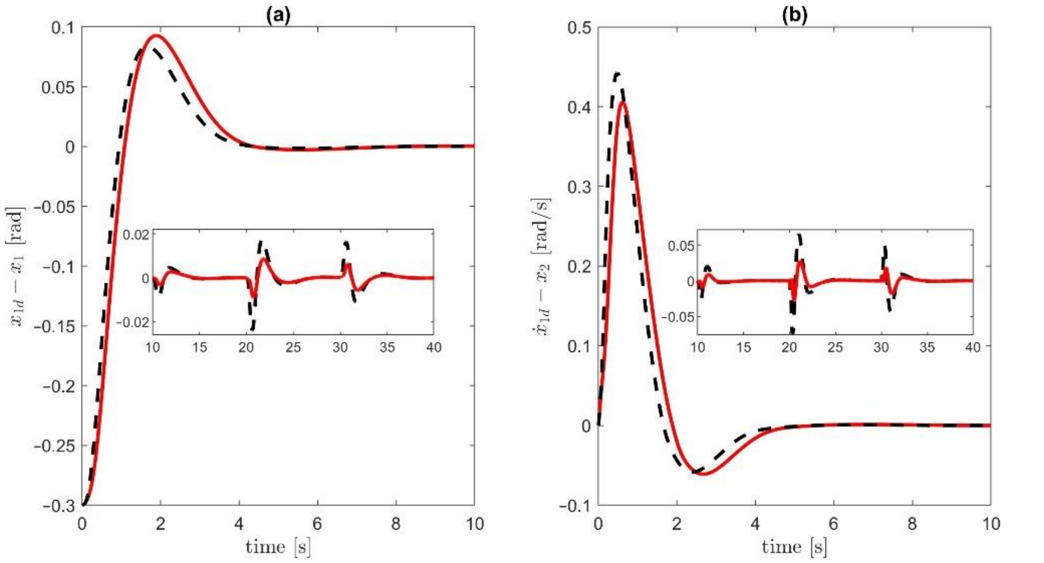

Figure 14. (**a**) Tracking error $x_{1d} - x_1$, (**b**) tracking error $\dot{x}_{1d} - x_2$. Dashed black line—$k_1 = k_2 = k_3 = k_4 = 5$, solid red line—$k_1 = k_2 = k_3 = k_4 = 15$.

The aim of the third experiment is to demonstrate the robustness of the proposed controller against the friction changes. The drive started knowing the actual values of the friction parameters. The reference position $x_{1d} = 0.3\sin(0.3t)$ is applied. At time $t = 50$ $[s]$, the actual values f_{s2} and f_{c2} were increased, achieving 130% of initial values ($f_{s2} = 19.5[Nm]$, $f_{c2} = 31$ $[Nm]$) and at $t = 100$ $[s]$, the real values f_{s4} and f_{c4} were increased to 110% of the initial values ($f_{s4} = 165[Nm]$, $f_{c4} = 440$ $[Nm]$). The simulation results obtained with $k_1 = k_2 = k_3 = k_4 = 5$ are presented in Figures 15 and 16.

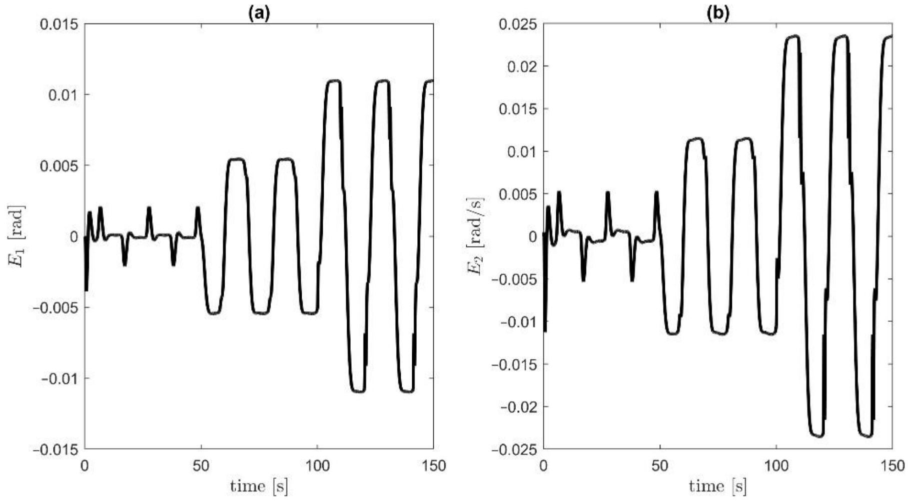

Figure 15. (**a**) Tracking error E_1, (**b**) tracking error E_2.

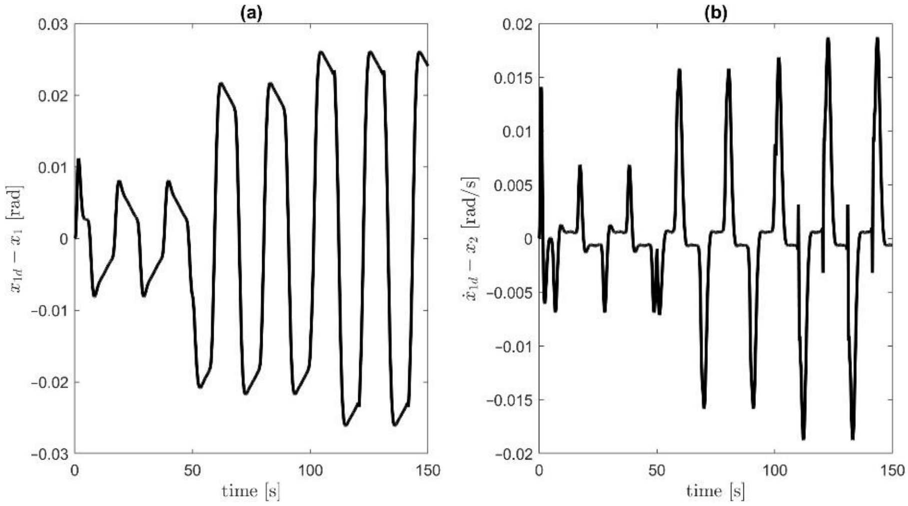

Figure 16. (**a**) Tracking error $x_{1d} - x_1$, (**b**) tracking error $\dot{x}_{1d} - x_2$.

Following the change of the actual friction parameters, the system remains stable. All tracking errors are bounded. As it may be expected, more differences between the actual and nominal parameters increase the tracking errors, but the tracking is still sufficiently accurate and fast.

The aim of the last experiment is to demonstrate the robustness of the proposed regulator to the unstructured disturbances $d_2(t)$ and $d_4(t)$, which represent the external disturbances, modelling inaccuracies, etc. The drive started knowing the actual values of all parameters. The reference position $x_{1d} = 0.3\sin(0.3t)$ is applied. The controller gains are $k_1 = k_2 = k_3 = k_4 = 5$. At time $t = 50$ $[s]$, the disturbance $d_2(t) = 4\sin(0.5t)$ appears. At $t = 150$ $[s]$, the disturbance $d_2(t)$ disappears and the disturbance $d_4(t) = 6\sin(0.1t)$ appears. Such disturbances are quite big, compared with the reference x_{1d} and $\dot{x}_{1d}$. The internal controller's tracking errors are presented in Figure 17a,b, while the resulting tracking errors $x_{1d} - x_1$, $\dot{x}_{1d} - x_2$ in Figure 18.

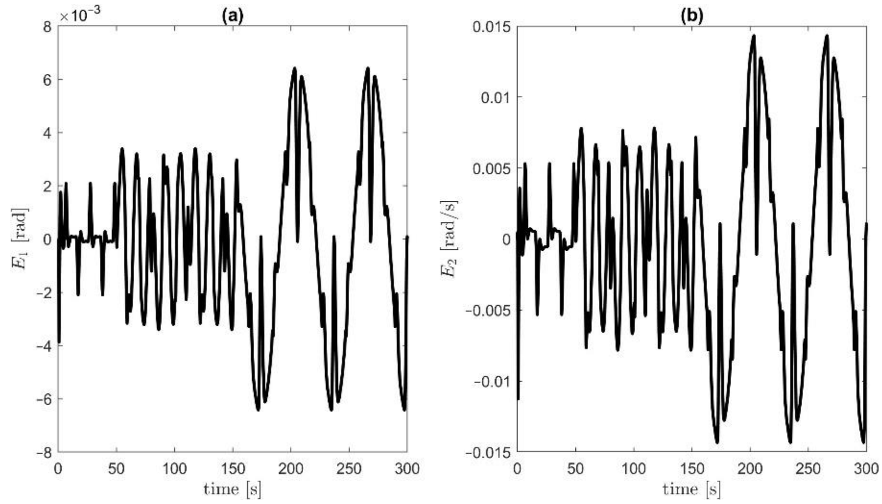

Figure 17. (**a**) Tracking error E_1, (**b**) tracking error E_2.

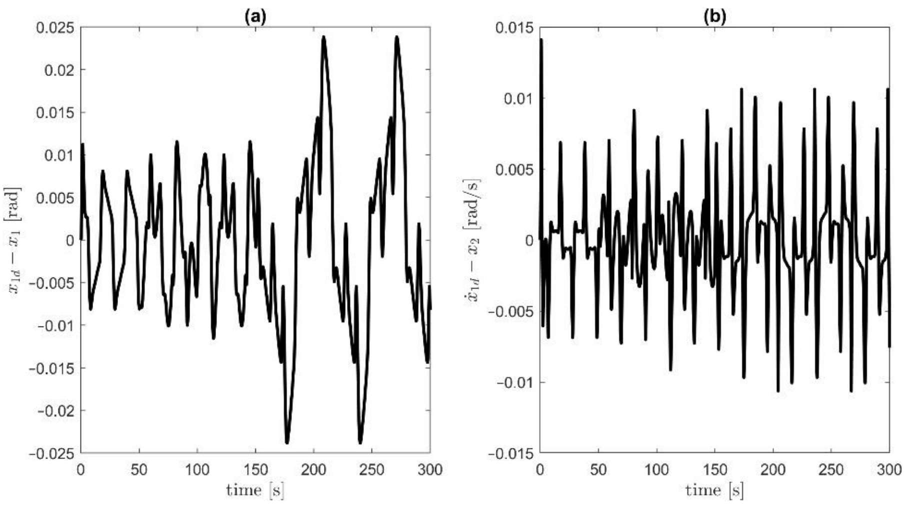

Figure 18. (**a**) Tracking error $x_{1d} - x_1$, (**b**) tracking error $\dot{x}_{1d} - x_2$.

Again, it is demonstrated that the proposed controller is robust against the external disturbances. When a disturbance occurs, the tracking error increases but remains bounded and the tracking accuracy is satisfactory.

6. Conclusions

A two-mass system considered here, was modelled by ordinary differential equations. A robust control approach was applied, which means that the nominal parameters were considered, and the system uncertainty represents a modelling gap between a nominal model and a real plant. The model includes nonlinear reactive torques, acting against the motion on both ends of a flexible shaft. Furthermore, the unstructured disturbances representing the external signals and modelling errors are included into the considered model. The only critical assumption concerning the model is that any uncertainty considered is bounded, however knowing the bound is not necessary. Thanks to this approach, the model used can be very general, flexible, and useful in numerous applications.

As the only measured signals are motor speed and position, an observer was necessary to control the load position effectively. Having considered several possibilities, a robust observer, based on the LMI solution, was designed to obtain the state estimation. It was formally proven that the estimation error is uniformly ultimately bounded (UUB), despite any bounded uncertainties. The observer design methodology was discussed and the impact of the design parameters on the observer performance was clearly established. The problem of testing several different algorithms to solve the LMI (16) will be the topic of further research.

A nonlinear controller was designed to cooperate with the observer and to assure sufficiently the accurate tracking of a desired position by the load. The controller was derived using a creative modification of backstepping. The control command filtering technique was used to avoid an 'explosion of complexity'. Finally, it was proven that the closed-loop observer-controller system trajectories are UUB despite any bounded uncertainties.

Several constraints on the state estimation errors and tracking errors, concerning the speed of convergence and the quasi-steady-state behavior, were derived. Although the obtained bounds are rather conservative, the derived formulae clearly indicate the influence of design parameters on the system performance. Therefore, the obtained controller, although containing 10 design parameters, is easy to tune.

Finally, the system performance was investigated by several examples concerning a huge manipulator. It was demonstrated that:

- the state estimations became accurate if the real system agrees with the model exactly,
- it is easy to obtain sufficiently accurate state estimations in the presence of any bounded parameter gap and bounded disturbances, by straightforward parameter tuning,
- the obtained closed-loop system tracks the desired load position sufficiently accurately and its UUB stability remains robust against the changes of parameters and the presence of bounded (but necessarily small) external disturbances, even if the reference trajectory is not smooth at the isolated points.

In summary, the problem of load position tracking by a two-mass system with incomplete state measurements was solved under a unique, never reported in references, set of assumptions. The proposed novel approach, connecting a robust, LMI-based technique to design an observer and a nonlinear controller derivation assuring the UUB stability, proved to be effective and comfortable and may be recommended for practical applications. The same observer-controller eliminates effectively two main difficulties occurring in a two-mass system control problem: the torsional oscillations of the flexible shaft and the degrading influence of the nonlinear friction or friction-like disturbance acting on both ends of the shaft.

A reliable study of the practical implementation of the described theory is left to the next paper. The obtained results make the practical implementation plans realistic, the controller is tunable and robust. The preliminary results are promising. The practical implementations depend on several factors neglected during the theoretical design, such as the sampling time, the digital position measurement, the digital speed calculation method, the unmodeled dynamics (inertia, delay) in propelling the torque generation, etc. The impact of all of these factors on the overall performance of the system is complicated. It is well known that some of them, such as increasing the sampling time, deteriorate the quality of the control. The control of so-called "imperfect systems" has been studied only recently and it has been noticed that in some electromechanical systems, it is possible to exploit the inevitable imperfections associated with the physical realizations, by stimulating the hidden dynamics associated with them [48]. For the discussed system, it may be the unmodeled dynamics of sensors and actuators. Thus, the problem remains complex, and the study of the qualitative and quantitative impacts of all of these factors on the system performance requires separate research and will be presented soon.

Author Contributions: Main idea, J.K. and P.M.; methodology, J.K. and P.M.; simulations, P.M.; validation, J.K.; writing—original draft preparation, J.K. and P.M.; writing—review, J.K.; visualization, P.M. All authors have read and agreed to the published version of the manuscript.

Funding: This research was funded by Politechnika Łódzka (Lodz University of Technology), subtask 1.1 of the task budget entitled: "Intensification of the publishing activity of employees, doctoral students and students of TUL by co-financing the OPEN ACCESS publication". The APC was funded by Politechnika Łódzka.

Data Availability Statement: Not applicable.

Conflicts of Interest: The authors declare no conflict of interest.

References

1. Peng, Y.; Cui, J.; Sun, J.; Zhang, M. Torsional Vibration for Rolling Mill with the Drive System Shaft Axis Deviations. *Arab. J. Sci. Eng.* **2021**, *46*, 12165–12177. [CrossRef]
2. Bortnowski, P.; Gładysiewicz, L.; Król, R.; Ozdoba, M. Models of Transverse Vibration in Conveyor Belt—Investigation and Analysis. *Energies* **2021**, *14*, 4253. [CrossRef]
3. Kim, T.; Lee, U.-K.; Kim, S.W.; Lim, H.; Kim, C.-W.; Cho, H.; Kang, K.-I. Flexible Double-Cage Hoist for High Operational Efficiency in Tall Building Construction. *Autom. Constr.* **2018**, *96*, 280–291. [CrossRef]
4. Guo, Y.; Zhang, D.; Zhang, X.; Wang, S.; Ma, W. Experimental Study on the Nonlinear Dynamic Characteristics of Wire Rope under Periodic Excitation in a Friction Hoist. *Shock Vib.* **2020**, *2020*, 8506016. [CrossRef]
5. Riane, R.; Doghmane, M.Z.; Kidouche, M.; Djezzar, S. Observer-Based H∞ Controller Design for High Frequency Stick-Slip Vibrations Mitigation in Drill-String of Rotary Drilling Systems. *Vibration* **2022**, *5*, 264–289. [CrossRef]
6. Chang, R.-I.; Lee, C.-Y.; Hung, Y.-H. Cloud-Based Analytics Module for Predictive Maintenance of the Textile Manufacturing Process. *Appl. Sci.* **2021**, *11*, 9945. [CrossRef]
7. Valenzuela, M.A.; Bentley, J.M.; Lorenz, R.D. Evaluation of Torsional Oscillations in Paper Machine Sections. *IEEE Trans. Ind. Appl.* **2005**, *41*, 493–501. [CrossRef]
8. Lu, G.; Zhou, J.; Cai, G.; Lv, L.; Fang, G. Active Vibration Control of a Large Space Antenna Structure Using Cable Actuator. *AIAA J.* **2021**, *59*, 1457–1468. [CrossRef]
9. Zhang, Y.; Zhang, M.; Fan, C.; Li, F. A Finite-Time Trajectory-Tracking Method for State-Constrained Flexible Manipulators Based on Improved Back-Stepping Control. *Actuators* **2022**, *11*, 139. [CrossRef]
10. Yang, H.; Wang, Z.; Zhang, T.; Du, F. A Review on Vibration Analysis and Control of Machine Tool Feed Drive Systems. *The Int. J. Adv. Manuf. Technol.* **2020**, *107*, 503–525. [CrossRef]
11. Awada, A.; Younes, R.; Ilinca, A. Review of Vibration Control Methods for Wind Turbines. *Energies* **2021**, *14*, 3058. [CrossRef]
12. Hua, Y.; Wang, S.; Li, B.; Bai, G.; Zhang, P. Dynamic Modeling and Anti-Disturbing Control of an Electromagnetic MEMS Torsional Micromirror Considering External Vibrations in Vehicular LiDAR. *Micromachines* **2021**, *12*, 69. [CrossRef] [PubMed]
13. Wang, C.; Liu, J.; Xin, L.; Li, G.; Pan, J. Design of Full-Order State Observer for Two-Mass Joint Servo System Based on the Fixed Gain Filter. *IEEE Trans. Power Electron.* **2022**, *37*, 10466–10475. [CrossRef]
14. Li, W.; Chen, L. Study on Modeling and Degradation Law of Transmission Efficiency for Harmonic Reducer. *J. Fail. Anal. Prev.* **2022**. [CrossRef]
15. Saldivar, B.; Mondié, S.; Ávila Vilchis, J.C. The Control of Drilling Vibrations: A Coupled PDE-ODE Modeling Approach. *Int. J. Appl. Math. Comput. Sci.* **2016**, *26*, 335–349. [CrossRef]
16. Di Meglio, F.; Aarsnes, U.J.F. A Distributed Parameter Systems View of Control Problems in Drilling. *IFAC-PapersOnLine* **2015**, *48*, 272–278. [CrossRef]
17. Saldivar, B.; Mondie, S.; Loiseau, J.J.; Rasvan, V. Stick-Slip Oscillations in Oillwell Drilstrings: Distributed Parameter and Neutral Type Retarded Model Approaches. *IFAC Proc. Vol.* **2011**, *18*, 284–289. [CrossRef]
18. Boussaada, I.; Mounier, H.; Niculescu, S.I.; Cela, A. Analysis of Drilling Vibrations: A Time-Delay System Approach. In Proceedings of the 2012 20th Mediterranean Conference on Control and Automation, MED 2012—Conference Proceedings, Barcelona, Spain, 3–6 July 2012; pp. 610–614. [CrossRef]
19. Lozynskyy, A.; Chaban, A.; Perzyński, T.; Szafraniec, A.; Kasha, L. Application of Fractional-Order Calculus to Improve the Mathematical Model of a Two-Mass System with a Long Shaft. *Energies* **2021**, *14*, 1854. [CrossRef]
20. Chaban, A.; Lis, M.; Szafraniec, A.; Jedynak, R. Application of Genetic Algorithm Elements to Modelling of Rotation Processes in Motion Transmission Including a Long Shaft. *Energies* **2021**, *14*, 115. [CrossRef]
21. Popenda, A.; Lis, M.; Nowak, M.; Blecharz, K. Mathematical Modelling of Drive System with an Elastic Coupling Based on Formal Analogy between the Transmission Shaft and the Electric Transmission Line. *Energies* **2020**, *13*, 1181. [CrossRef]
22. Szabat, K.; Orlowska-Kowalska, T. Vibration Suppression in a Two-Mass Drive System Using PI Speed Controller and Additional Feedbacks—Comparative Study. *IEEE Trans. Ind. Electron.* **2007**, *54*, 1193–1206. [CrossRef]
23. Orlowska-Kowalska, T.; Dybkowski, M.; Szabat, K. Adaptive Sliding-Mode Neuro-Fuzzy Control of the Two-Mass Induction Motor Drive Without Mechanical Sensors. *IEEE Trans. Ind. Electron.* **2010**, *57*, 553–564. [CrossRef]
24. Serkies, P.J.; Szabat, K. Application of the MPC to the Position Control of the Two-Mass Drive System. *IEEE Trans. Ind. Electron.* **2013**, *60*, 3679–3688. [CrossRef]
25. Derugo, P.; Szabat, K.; Pajchrowski, T.; Zawirski, K. Fuzzy Adaptive Type II Controller for Two-Mass System. *Energies* **2022**, *15*, 419. [CrossRef]
26. Kamiński, M.; Szabat, K. Adaptive Control Structure with Neural Data Processing Applied for Electrical Drive with Elastic Shaft. *Energies* **2021**, *14*, 3389. [CrossRef]

27. Kabziński, J.; Mosiołek, P. Adaptive Control of Nonlinear Resonant Systems with Damping. In Proceedings of the 2015 20th International Conference on Methods and Models in Automation and Robotics (MMAR), Miedzyzdroje, Poland, 24–27 August 2015; pp. 659–664.
28. Kabziński, J. Adaptive Control of Drillstring Torsional Oscillations. *IFAC-PapersOnLine* **2017**, *50*, 13360–13365. [CrossRef]
29. Kabziński, J.; Mosiołek, P. Integrated, Multi-Approach, Adaptive Control of Two-Mass Drive with Nonlinear Damping and Stiffness. *Energies* **2021**, *14*, 5475. [CrossRef]
30. Inoue, Y.; Katsura, S. Spatial Disturbance Suppression of a Flexible System Based on Wave Model. *IEEJ J. Ind. Appl.* **2018**, *7*, 236–243. [CrossRef]
31. Wicher, B.; Brock, S. Tuning Optimization of Extended State Observer for Two Mass System with Elastic Joint and Backlash. In Proceedings of the 2018 18th International Conference on Mechatronics—Mechatronika (ME), Brno, Czech Republic, 5–7 December 2018; pp. 1–6.
32. Dróżdż, K.; Szabat, K. Application of Unscented Kalman Filter in Adaptive Control Structure of Two-Mass System. In Proceedings of the 2016 IEEE International Power Electronics and Motion Control Conference (PEMC), Varna, Bulgaria, 25–28 September 2016; pp. 1150–1154. [CrossRef]
33. Yokoyama, M.; Oboe, R.; Shimono, T. Robustness Analysis of Two-Mass System Control Using Acceleration-Aided Kalman Filter. In Proceedings of the IECON 2018—44th Annual Conference of the IEEE Industrial Electronics Society, Washington, DC, USA, 21–23 October 2018; pp. 4600–4605. [CrossRef]
34. Serkies, P. Estimation of State Variables of the Drive System with Elastic Joint Using Moving Horizon Estimation (MHE). *Bull. Pol. Acad. Sci. Tech. Sci.* **2019**, *67*, 883–892. [CrossRef]
35. Szabat, K.; Tokarczyk, A.; Wróbel, K.; Katsura, S. Application of the Multi-Layer Observer for a Two-Mass Drive System. In Proceedings of the 2020 IEEE 29th International Symposium on Industrial Electronics (ISIE), Delft, The Netherlands, 17–19 June 2020; pp. 265–270. [CrossRef]
36. Szabat, K.; Wróbel, K.; Śleszycki, K.; Katsura, S. States Estimation of the Two-Mass Drive System Using Multilayer Observer. In Proceedings of the 2021 IEEE 19th International Power Electronics and Motion Control Conference (PEMC), Gliwice, Poland, 25–29 April 2021; pp. 743–748. [CrossRef]
37. Sieklucki, G. Optimization of Observers in a Two-Mass System—Dual LQ Problem. In Proceedings of the 2018 International Symposium on Electrical Machines (SME), Andrychów, Poland, 10–13 June 2018; pp. 1–6. [CrossRef]
38. Kabziński, J.; Mosiołek, P. Adaptive, Observer-Based Synchronization of Different Chaotic Systems. *Appl. Sci.* **2022**, *12*, 3394. [CrossRef]
39. Dimassi, H.; Said, S.H.; Loria, A.; M'Sahli, F. An Adaptive Observer for a Class of Nonlinear Systems with a High-Gain Approach. Application to the Twin-Rotor System. *Int. J. Control* **2021**, *94*, 370–381. [CrossRef]
40. Pourgholi, M.; Majd, V.J. An LMI-Based Adaptive Resilient Observer Design for a Class of Nonlinear Systems. In Proceedings of the 2009 IEEE Control Applications, (CCA) & Intelligent Control, (ISIC), St. Petersburg, Russia, 8–10 July 2009; pp. 643–647. [CrossRef]
41. Chen, M.-S.; Chen, C.-C. Robust Nonlinear Observer for Lipschitz Nonlinear Systems Subject to Disturbances. *IEEE Trans. Automat. Control* **2007**, *52*, 2365–2369. [CrossRef]
42. Bo, T.X.; Ohishi, K.; Miyazaki, T.; Yokokura, Y. Sensor-Less Torque Control Considering Contact Phase for Two-Mass System. In Proceedings of the 2018 IEEE 15th International Workshop on Advanced Motion Control (AMC), Tokyo, Japan, 9–11 March 2018; pp. 687–692. [CrossRef]
43. Pennestrì, E.; Rossi, V.; Salvini, P.; Valentini, P.P. Review and Comparison of Dry Friction Force Models. *Nonlinear Dyn.* **2016**, *83*, 1785–1801. [CrossRef]
44. Kabziński, J.; Mosiołek, P. *Projektowanie Nieliniowych Układów Sterowania (Nonlinear Control Design)*; PWN SA: Warszawa, Poland, 2018; ISBN 978-83-01-19697-4.
45. Nesterov, Y.; Nemirovskii, A. *Interior-Point Polynomial Algorithms in Convex Programming*; Society for Industrial and Applied Mathematics: Philadelphia, PA, USA, 1994. [CrossRef]
46. Swaroop, D.; Hedrick, J.K.; Yip, P.P.; Gerdes, J.C. Dynamic Surface Control for a Class of Nonlinear Systems. *IEEE Trans. Automat. Control* **2000**, *45*, 1893–1899. [CrossRef]
47. Yuan, X.; Chen, B.; Lin, C. Prescribed Finite-Time Adaptive Neural Tracking Control for Nonlinear State-Constrained Systems: Barrier Function Approach. *IEEE Trans. Neural. Netw. Learn Syst.* **2021**, 1–10. [CrossRef]
48. Bucolo, M.; Buscarino, A.; Famoso, C.; Fortuna, L.; Frasca, M. Control of imperfect dynamical systems. *Nonlinear Dyn.* **2019**, *98*, 2989–2999. [CrossRef]